筑　波　大　学

博　士　（医学）　学　位　論　文

Rev-erb agonist improves adverse cardiac remodeling and survival in myocardial infarction through an anti-inflammatory mechanism

(Rev-erb アゴニストは 抗炎症機序を介して 心筋梗塞における 心リモデリングと生存率を改善する)

2017

筑波大学大学院博士課程人間総合科学研究科

Endin Nokik Stujanna

Table of Contents

Abbreviations

AMPK	Activated Protein Kinase
BW	Body Weight
CD11b	Cluster of Differentiation 11 b
CD206	Cluster of Differentiation 206
CD45	Cluster of Differentiation 45
DAPI	4',6-diamidino-2-phenylindole
DNA	deoxyribonucleic acid
FITC	Fluorescein Isothiocyanate
HBSS	Hank's Balanced Salt Solution
IBM	International Business Machines
IgG	Immunoglobulin G
IL-6	Interleukin-6
LAD	Left Anterior Descending
LDL	Low Density Lipoprotein
LV	Left Ventricular
LVDd	Left Ventricular end diastolic Diameter

LVDs	Left Ventricular end systolic Diameter
LVEF	Left Ventricular Ejection Fraction
LVs	Left Ventricles
Ly6g	Lymphocyte antigen 6 complex locus G6D
MΦ	Macrophage
MACS	Magnetic-activated cell sorting
Mcp-1	Monocyte chemoattractant protein-1
MI	Myocardial Infarction
MI+SR	Myocardial Infarction + SR9009
MI+V	Myocardial Infarction + Vehicle
MMP-9	Matrix Metallopeptidase-9
MMPs	Matrix Metalloproteinases
mRNA	Messenger Ribonucleic Acid
Nppb	Natriuretic peptide precursor B
NR1D1	Nuclear Receptor 1 group D 1
NR1D2	Nuclear Receptor 1 group D 2
PBS	Phosphate Buffered Saline
PCR	Polymerase chain reaction
PGC-1	Proliferator-Activated Receptor-

	Gamma Coactivator-1
PPAR	Peroxisome Proliferator Activated Receptor
RNA	Ribonucleic Acid
SEM	standard error of the mean
Sham+SR	Sham + SR9009
Sham+V	Sham +Vehicle
Sirt1	Sirtuin 1
SPSS	Statistical Package for the Social Sciences
TFAM	Transcription Factor A Mitochondrial
VO2	Volume Oxygen

Chapter 1 Introduction

1.1 Background

As a leading cause of death and an increasing health burden worldwide, myocardial infarction (MI) remains one of the most important clinical entities. After the onset of MI, the left ventricle (LV) undergoes a continuum of molecular, cellular, and extracellular responses that result in LV wall thinning, dilatation, and dysfunction (Thygesen et al., 2012). The cardiac healing and remodeling process after MI can be divided into four phases: the death of cardiomyocytes, acute inflammation, the formation of granulation tissue, and scar formation (Figure 1). Acute inflammation usually occurs just after the onset of myocardial infarction. During this phase, neutrophils and monocytes are recruited into necrotic tissue, and they release inflammatory cytokines and matrix metalloproteinase (MMP) (Liehn et al., 2011). Inflammatory cell infiltration and MMP production play important roles in the degradation of necrotic debris and the subsequent scar formation. However, excess inflammatory response and MMP overproduction are likely to induce adverse cardiac remodeling,

leading to left ventricular dilatation, dysfunction, and cardiac rupture (Frangogiannis, 2015; Matsui et al., 2010). Despite the significant progress made on therapeutic strategies for MI in last few decades, mortality and morbidity remain high, and adverse cardiac remodeling after MI remains a critical issue to be solved. Therefore, continuous improvement in medications for the disease is still a major concern in global medical research.

Nuclear receptors (NRs) are members of a large superfamily and widely considered as ligand-activated transcriptional factors. These were originally found within cells that are responsible for sensing steroid and thyroid hormones and certain other molecules, and work with other proteins to regulate the expression of specific genes, thereby controlling the development, homeostasis, and metabolism of the organism (Chambon, 2005; Evans, 2005). Nuclear receptors represent one of the most important targets for therapeutic drug development, and many compounds targeted for nuclear receptors have already been developed as marketable drugs, e.g. peroxisome proliferator-activated receptor α and γ activators.

Rev-erb belongs to a nuclear receptor superfamily, and contains two subgroups, Rev-erb α (NR1D1) and β (NR1D2). Rev-erb α is highly expressed in the liver, skeletal muscle, adipose tissue, heart and brain,

participating in the development and circadian regulation of these tissues. (Solt et al., 2012). Rev-erb β displays a similar structure and has been implicated in the control of lipid and glucose metabolism and circadian rhythm, collaborating extensively with Rev-erb α (Bugge et al., 2012). Heme was identified as a physiological ligand for Rev-erb receptor, which regulates their transcriptional activity (Figure 2). Moreover, Rev-erb α displays a hydrophobic interface that binds the corepressor N-CoR, making it a potent transcriptional repressor (Solt et al., 2012; Woldt et al., 2013). Previous studies reported Rev-erb α regulated mitochondrial biogenesis in loss- and gain-of-function settings. Rev-erb α deficiency in skeletal muscle resulted in reduced mitochondrial content and ATP production through deactivating AMPK-SIRT1–PGC1 signaling pathway (Woldt et al., 2103). Recently, SR9009 and SR9011 were developed as synthetic Rev-erb agonists, which facilitates Rev-erb α to recruit its corepressor NCoR and repress downstream targets (Solt et al., 2012). From the results of the previous studies using agonists, it has been identified that the nuclear receptor Rev-erb α plays a pivotal role in the modulation of skeletal muscle oxidative capacity by regulating mitochondrial biogenesis and autophagy, leading to increasing in exercise capacity (Woldt et al., 2013). Moreover, long-term treatment with SR9009 was shown to reduce atherosclerotic

plaque by decreasing the ratio of proinflammatory M1 macrophages to anti-inflammatory M2 macrophages in low-density lipoprotein (LDL) receptor-deficient mice fed a Western diet (Sitaula et al., 2015). Therefore, Rev-erb is expected to be a promising therapeutic target for metabolic syndrome and atherosclerotic disease. However, little is known about the Rev-erb agonist effect on the progression of MI and heart failure.

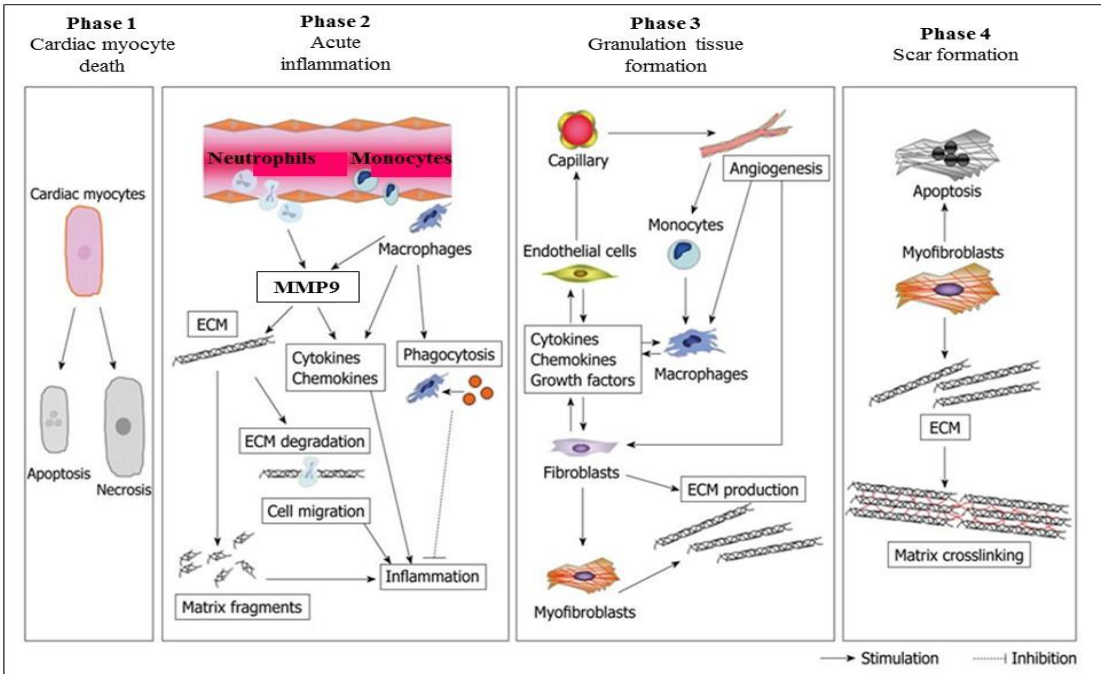

Figure 1. Phases of cardiac healing and remodeling process after MI: (1) death of cardiomyocytes; (2) acute inflammation; (3) formation of granulation tissue; and (4) scar formation.

Death of cardiomyocytes starts at approximately 1 h after coronary artery occlusion, and can either be the result of apoptosis or necrosis. During acute inflammation, the influx of inflammatory cells, including neutrophils and monocytes, for phagocytosis and removal of dead cardiomyocytes into the infarcted area and degradation of the extracellular matrix (ECM) by matrix metalloproteinase (MMP) takes place between 1 h and 4 d after MI. MMP also modulates inflammatory cytokine and chemokine activity. Generation of matrix fragments exerts potent inflammatory effects. Thereafter, formation of granulation tissue, characterized by the presence of fibroblasts, macrophages, myofibroblasts, new blood vessels, and ECM proteins, occurs in the infarcted heart between 2 and 14 d after MI. To rescue the loss of the shielding effects of the normal matrix, fibroblasts and myofibroblasts produce ECM. Finally, granulation tissue matures in the infarcted heart between 14 d and 2 mo after MI. The scar is characterized by a cross-linked, collagen-rich region that is induced by lysyl oxidase. In this phase, most infarct myofibroblasts undergo apoptosis and disappear. The time intervals for each phase are dependent on the species. (Matsui et al., 2010)

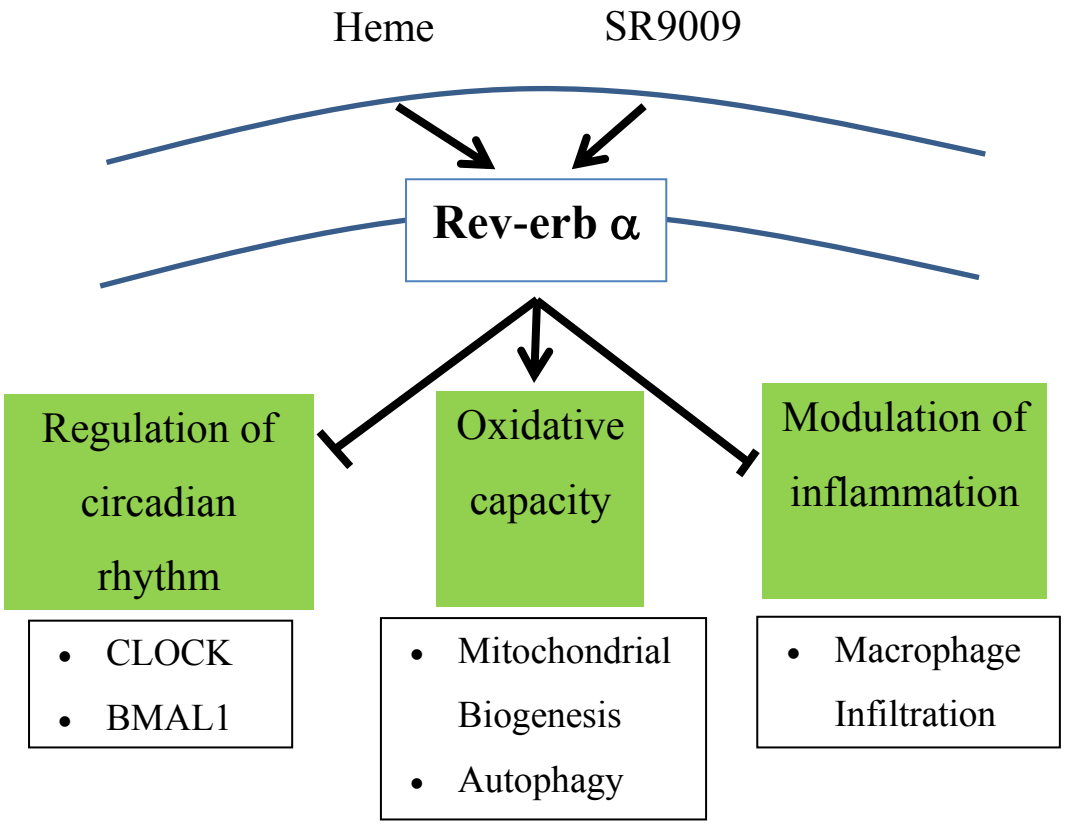

Figure 2. Schematic of Rev-erb α receptor.
Heme was identified as a physiological ligand for Rev-erb receptor. Recently, SR9009 is developed as a synthetic Rev-erb agonist. The nuclear receptor Rev-erb α plays a key role in (1) regulation of circadian rhythm (2) modulation of skeletal muscle oxidative capacity by regulating mitochondrial biogenesis and autophagy, and (3) modulation of inflammatory response through macrophage infiltration.

1.2 Objective

This study was aimed to clarify the roles of Rev-erb in post-MI remodeling and the effects of Rev-erb agonist SR9009 on cardiac function and survival after MI.

Chapter 2 Methods

2.1 Mouse Model

After receiving approval from the Institutional Animal Experiment Committee of the University of Tsukuba, animal experiments were carried out humanely and in accordance with the Guide for the Care and Use of Laboratory Animals published by the US National Institutes of Health, the Regulation for Animal Experiments in our university, and the Fundamental Guideline for Proper Conduct of Animal Experiment and Related Activities in Academic Research Institutions under the jurisdiction of the Ministry of Education, Culture, Sports, Science and Technology of Japan.

We used 165 male wild-type C57BL6 mice purchased from CLEA Japan, Inc. (Tokyo, Japan) in total. At 12-14 weeks of age, mice were anesthetized with ketamine and xylazine, followed by tracheal intubation and artificial ventilation (MiniVent 845; Harvard Apparatus, Holliston, MA, USA). Next, a thoracotomy was performed to expose the heart, and MI was induced by the permanent ligation of the left anterior descending coronary artery (LAD) with 7-0 polypropylene suture passed about 1 mm

from the inferior margin of the left atrial auricle. MI was confirmed by visual observation of myocardial color change and ST-segment elevation on the electrocardiogram recording. The sham-operated group was subjected to a similar procedure without ligation of the coronary artery. After closure of the thorax and recovery of spontaneous breathing, the mice were extubated and placed in a new box on the warm pad for recovery (Figure 3). Study period was within 2 weeks after surgery, and mice were monitored daily during the study. Among 165 mice used for all experiments, 58 mice died before sacrifice (40 mice died due to heart failure and/or arrhythmia including operational death, and 18 died due to cardiac rupture). If mice showed body weight loss of more than 20% and/or significant clinical signs due to the development of heart failure (e.g., increased respiratory rates, reduced activity, piloerection, hunched posture), they were immediately euthanized by intraperitoneal injection of 200 mg/kg sodium pentobarbital. Four mice were euthanized because of cardio-respiratory distress (weakness, fatigue, deep breathing, dyspnea). Thus, euthanized mice were considered as death due to heart failure.

SR9009 was purchased from Merck Millipore (Darmstadt, Germany) and was dissolved in 1% dimethyl sulfoxide (DMSO) in normal saline. SR9009 could administrated via injection or oral and no side effect are

reported. We started intraperitoneal administration with SR9009 (100 mg/kg/day or vehicle (1% DMSO in normal saline) from 1 day before surgery. Consequently, mice were divided into four groups: sham-operated mice treated with vehicle (Sham+V), sham-operated mice treated with SR9009 (Sham+SR), MI mice treated with vehicle (MI+V), and MI mice treated with SR9009 (MI+SR). The selection of the doses was based on the previous study and displayed no apparent toxicity (Sitaula et al., 2015). We first investigated mortality over the 14 days after MI and performed echocardiography at 7 days after MI and just before sacrifice. Next, we excised and collected the hearts of the mice sacrificed at 3 and 7 days after surgery for RNA extraction and histochemical analysis, and those of the mice sacrificed at 1 and 5 days after surgery for flow cytometric analysis (Figure 4).

2.2 Echocardiography

This study obtained echocardiographic images from the parasternal long-axis view and short-axis view at the papillary muscle level under anesthesia with isoflurane using a Doppler echocardiographic system (Vevo 2100; Visual Sonics, Toronto, Canada). Accordingly, we determined the heart

rate, left ventricular (LV) end-diastolic diameter (LVDd), LV end-systolic diameter (LVDs), fractional shortening (FS), LV ejection fraction (LVEF), interventricular septal thickness (IVST), posterior wall thickness (PWT) and LV mass. EF was calculated by the Teichholz method.

2.3 RNA Gene Expression

RNA extraction and gene expression analysis were performed as previously described with minor modifications (Xu et al., 2012). In brief, total RNA was extracted from the LV tissues using a RNeasy Fibrous Tissue Mini Kit (Qiagen, Venlo, Netherlands), and 2 μg of total RNA was reverse transcribed to cDNA with a High-Capacity cDNA Reverse Transcription Kit (Thermo Fisher Scientific, Inc., Waltham, MA, USA). The mRNA expression levels of the target genes were analyzed by an ABI Prism 7500 sequence detection system (Thermo Fisher Scientific). The commercially available gene-specific primers and probe sets were obtained from Integrated DNA Technologies (Coralville, IA, USA). The PCR mixture (10 μl total volume) consisted of primer and probe for each gene at 250 nM, and PrimeTime Gene Expression Master Mix (Integrated DNA Technologies). PCR amplification was performed in duplicate as follows: 1

cycle at 95°C for 10 min and 40 cycles at 94°C for 15 s and 60°C for 1 min. The primer and probe used in the study are mentioned as follows: *Nr1d1* (Mm.PT.58.17472803), *Nr1d2* (Mm.PT.58.31165809), *Nppb* (Mm.PT.58.8584045.g), *Il6* (Mm.PT.58.10005566), *Mcp1* (Mm.PT.58.42151692), *Ly6g* (Mm.PT.58.30498043), *Itgam* (*Cd11b*) (Mm.PT.5814195622), *Mmp9* (Mm.PT.58.10100097), *Col1a1* (Mm.PT.58.756.2513), *Col3a1* (Mm.PT.58.13848686). The quantitative values of target mRNA were normalized by 18S rRNA (4319413E, Thermo Fisher Scientific) expression. The results were obtained from 2-3 independent measurements (n=4 in each group) performed in duplicate.

2.4 Enzyme Immunoassay (EIA) for BNP

Plasma BNP concentration was measured by using a Brain Natriuretic Peptide EIA Kit (RAB0386-1KT, Sigma-Aldorich, Inc., St. Luise, MO, USA) according to the procedural manual. In brief, the samples and standards mixed with 10 pg/ml of biotinylated BNP peptide were added to the anti-BNP antibody-immobilized plate, where the biotinylated BNP peptide competed with unlabeled (endogenous) BNP for binding to the antibody. After incubating plate at 4°C overnight and washing wells,

horseradish peroxidase (HRP)-streptavidin solution was added to each well, and incubated for 45 minutes at room temperature. After washing, tetramethylbenzidine (TMB) solution was then added to each well to visualize the immunoreaction. After adding stop solution, absorbance of each well was measured by using Varioskan LUX microplate reader (ThermoFisher) at 450nm. The result was obtained from one measurement (n=4 in each group) performed in duplicate.

2.5 Histology and Immunofluorescence

The hearts were fixed with 4% paraformaldehyde, embedded in paraffin, sectioned into 4-μm-thick slices, and stained with Masson's trichrome. Images were obtained by a digital microscope (Biozero BZ-X700; Keyence, Osaka, Japan), and collagen deposition was calculated by dividing the collagen depositing area to the total area. The analysis was performed using ImageJ analysis software (Ver. 1.45, NIH, USA).

To evaluate the expression of MMP9 and Rev-erb α, we performed immunofluorescence. After deparaffinization and antigen activation, sections were incubated with polyclonal rabbit anti-MMP9 (ab38898; Abcam, Cambridge, UK) or Rev-erb α (sc-100910, Santa Cruz

Biotechnology, Inc, Dallas, TX, USA) antibodies at 4°C overnight. Next, sections were sufficiently rinsed in PBS and then incubated to Alexa Fluor 594-labeled goat anti-rabbit IgG or Alexa Fluor 488-labeled goat anti-mouse IgG (Thermo Fisher Scientific) at room temperature for 2 hours. After rinsing in PBS and mounting on slides with mounting medium with DAPI, the fluorescent images were captured by a digital fluorescent microscope (Biozero BZ-X700). The ratio of Alexa Fluora 594-positive area to total area was calculated with the ImageJ analysis software.

2.6 Flow Cytometry

Heart inflammatory cells were isolated and processed as described previously (Machino-Ohtsuka et al., 2014). In brief, 1 and 5 days after MI or sham operation, hearts were excised, cut roughly, and dissociated by using gentleMACS Dissociator (Miltenyi Biotec, Bergisch Gladbach, Germany) in HBSS mixed with hyaluronidase, collagenase, and DNase I in accordance with the experimental protocol. Next, the cells were rinsed with PBS, dissolved with MACS buffer (Miltenyi Biotec), and passed through cell strainer (70μm) (Corning Inc., Corning, NY, USA). After removing red blood cells by ACK buffer, the cells were directly stained with

fluorescence-conjugated antibodies as follows: FITC-conjugated anti-mouse Ly6g antibody, PE-conjugated anti-mouse CD11b antibody, and APC-conjugated anti-mouse CD45.2 antibody. To differentially investigate M1/M2 macrophages, the cells collected from mice 5 days after surgery were also stained with FITC-conjugated anti-mouse F4/80 antibody, PE-conjugated anti-mouse CD11b antibody, and APC-conjugated anti-mouse CD206 antibody. After 1 hour incubation at 37°, the cells were rinsed with PBS, diluted with MACS buffer, mixed with DAPI, and analyzed with a FACSCalibur instrument (Becton Dickinson Co., Franklin Lakes, NJ), followed by analysis with FlowLogic software (Inivai Technologies, Mentone, Victoria, Australia). All antibodies were obtained from Bay Bioscience (Brookline MA, USA), Biolegend Inc. (San Diego, CA, USA), or Amersham Biosciences Corp. (Buckinghamshire, United Kingdom).

2.7 Western Blotting Analysis

Western blotting was performed as described previously (Xu et al., 2012). In brief, isolated LVs were homogenized in PRO-PREP protein extraction solution (iNtRON Biotechnology, Inc. Kyungki-Do, Korea), and the supernatants were used for western immunoblotting. Appropriate volumes

of the samples (10 μg) were mixed with an equal volume of sample buffer, heated at 95°C for 5 min, and then subjected to SDS-PAGE using 4-15% gradient polyacrylamide gels (Bio-Rad Laboratory, Hercules, CA, USA). The proteins were transferred by semidry electroblotting from gels to polyvinylidene difluoride membranes. The blots were then blocked with the primary antibodies as follows: phospho-NF-κB p65 (Ser536 (#3033) and Ser468 (#3039)), NF-κB (L8F6) (#6956), phospho-p38 (Thr180/182) (#9211S), p38 mitogen activated protein kinase (MAPK) (#9212), phospho-p44/42 MAPK (Thr202/Thr204) (#9101S), p44/42 MAPK (#9102), β-actin (#4967) (all were purchased from Cell Signaling Technology, Inc., Danvers, MA, USA), and Rev-erb α (RS-14) (sc-100910, Santa Cruz Biotechnology, Inc, Dallas, TX, USA). The blots were incubated with an appropriate second antibody, horseradish peroxidase (HRP)-conjugated goat anti-rabbit IgG (ab6721, Abcam) or HRP-conjugated rabbit anti-mouse IgG (ab97046, Abcam). Immunoreactions were visualized with an enhanced chemiluminescence method (ECL Prime Western Blotting Detection; GE Healthcare, Southeast, UK). Densitometric analysis was performed on scanned immunoblot images with the ImageJ analysis software. The ratios of densities of bands detected by using phosphorylated antibodies to those detected by using nonphosphorylated

(total) antibodies or β-actin antibody was obtained from 2-3 independent measurements (n = 3 per group for each measurement).

2.8 Statistical Analysis

All data are expressed as means ± SEM. Experimental groups were compared by one-way analysis of variance followed by Bonferroni's test for multiple comparisons. When the results were not normally distributed, statistical analyses were performed using Kruskal-Wallis one-way analysis of variance. The effect of SR9009 on the survival of mice was analyzed by Kaplan-Meier methods and compared by log-rank test. Differences were considered statistically significant at $p < 0.05$. The analysis was performed using IBM SPSS version 21.0 software (IBM Co., Armonk, NY, USA).

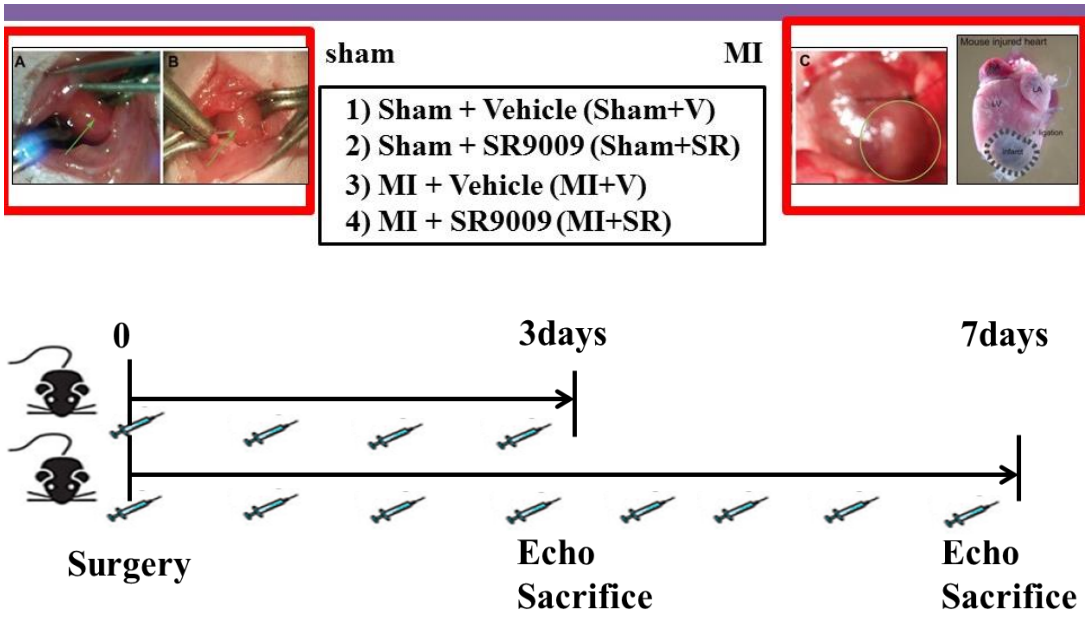

Figure 3. Animals model and study protocol.
Intraperitoneal administration with SR9009 (100 mg/kg/day or vehicle (1% DMSO in normal saline) was started on 1 day before surgery. Mice were divided into four groups: 1) sham-operated mice treated with vehicle (Sham+V), 2) sham-operated mice treated with SR9009 (Sham+SR), 3) MI mice treated with vehicle (MI+V), and 4) MI mice treated with SR9009 (MI+SR). MI was induced by the permanent ligation of the left anterior descending coronary artery (LAD) with 7-0 polypropylene suture passed about 1 mm from the inferior margin of the left atrial auricle. MI was confirmed by visual observation of myocardial color change and ST-segment elevation on the electrocardiogram recording. The sham-operated group was subjected to a similar procedure without ligation of the coronary artery.

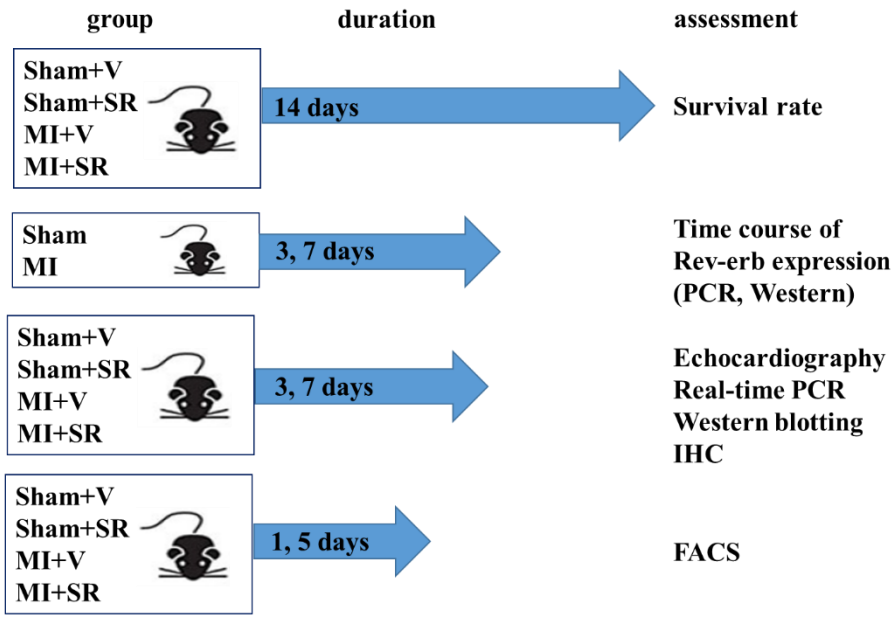

Figure 4. Assesment protocol.
Survival rate was monitored over the 14 days after MI. Echocardiographic analysis was performed on 7 days after surgery. For RT-PCR, western blotting, and immunofluorescence, hearts were collected on 3 and 7 days after surgery. For flow cytometry, hearts were collected on 1 and 5 days after surgery.

Chapter 3 Results

3.1 Gene and protein expression levels of *Rev-erb* in the LVs after MI

First, we investigated the gene and protein expressions of *Rev-erb* in the LVs after MI. The mRNA expression level of *Rev-erb α* in the LVs was slightly changed but not significantly different between sham, day 3, and day 7 after MI (Figure 5A). Moreover, the expression level of *Rev-erb β* mRNA in the LV was significantly decreased 3 and 7 days after MI (Figure 5B).

The protein expression level of Rev-erb α was slightly increased on day 3 whereas it was significantly decreased on day 7 after MI (Figure 6).

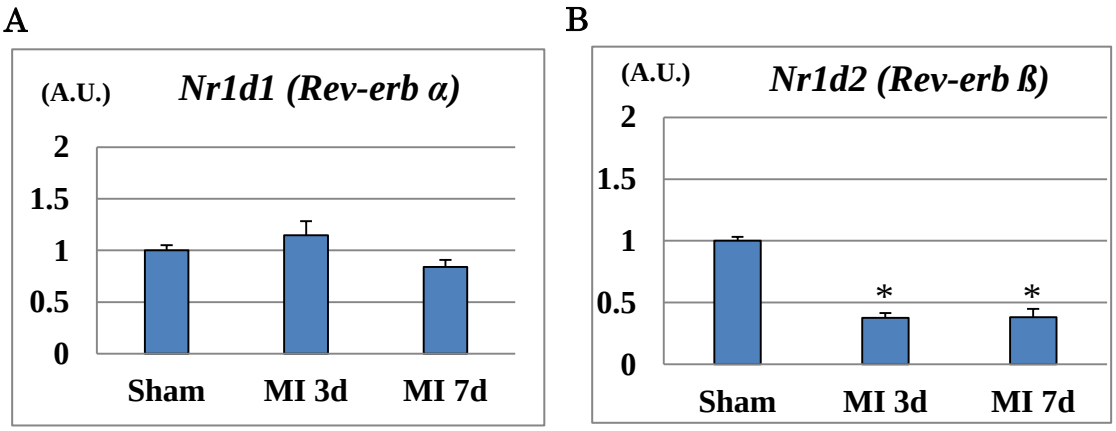

Figure 5. mRNA expression levels of *Rev-erb α* (A) and *β* (B) in the left ventricular border area after myocardial infarction.

(A) The expression level of *Rev-erb α* mRNA in the LV was not significantly different between sham, 3 days, and 7 days after MI (n=4 animals for each time point). (B) The expression level of *Rev-erb β* mRNA in the LV was significantly decreased 3 and 7 days after MI (n=4 animals for each time point). The bar graphs show the group mean±SEM. **p*<0.05 vs Sham.

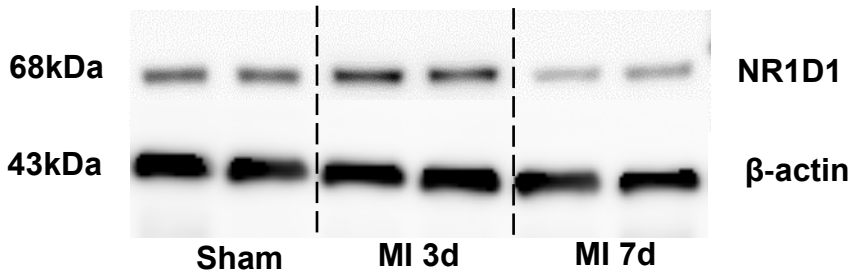

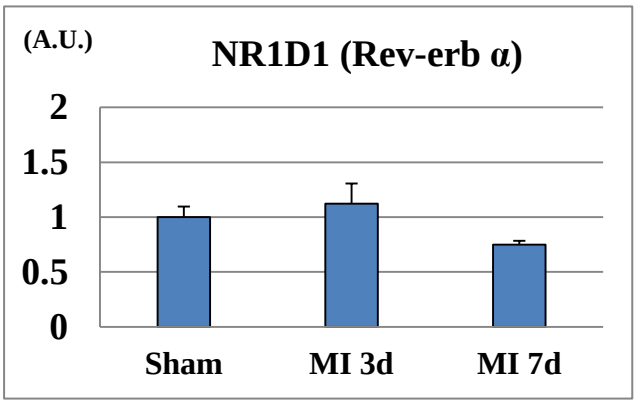

Figure 6. Protein expression level of Rev-erb α in the in the left ventricular border area after myocardial infarction.
Western blotting analysis showed a significant decrease in the expression level of Rev-erb α 7 days after MI (n=3 animals for each time point). The bar graphs show the group mean±SEM. **p*<0.05 vs Sham.

3.2 Survival rate after MI

We evaluated survival after MI with or without SR9009 treatment. After permanent ligation of the LAD in 58 mice (38 in MI+V; 20 in MI+SR), 18

mice (15 in MI+V; 3 in MI+SR) died because of ventricular rupture that occurred between 3 and 7 days after MI. Meanwhile, 16 mice (11 in MI+V; 5 in MI+SR) died without bleeding in the thoracic cavity. We assumed they died either due to acute heart failure or cardiac arrhythmia. Survival rate was markedly reduced by 31.6% in MI+V. However, it was significantly higher in MI+SR (60.0%, at day 14 after myocardial infarction; log-rank test, p=0.032 compared between MI+SR and MI+V; Figure 7).

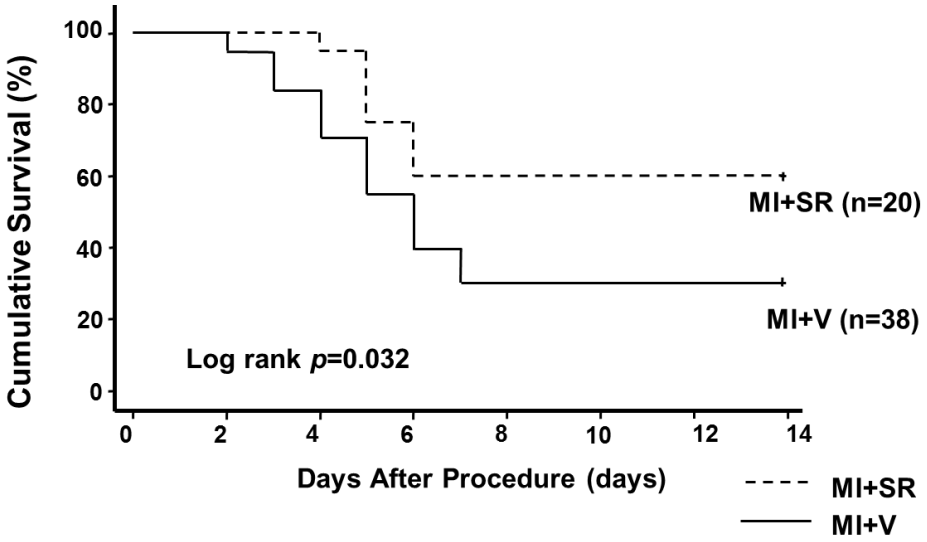

Figure 7. Kaplan-Meier survival curves after myocardial infarction. Survival rate was significantly higher in MI+SR than in MI+V (60.0% vs 31.6% at day 14 after myocardial infarction; log-rank test, p=0.032 compared between MI+SR and MI+V).

3.3 Echocardiographic analysis

To assess cardiac function after MI, we performed echocardiographic

analysis 7 days after surgery in each group (Figure 8). SR9009 treatment significantly improved LVEF and FS (Table). LVDd, Ds, and LV mass were slightly lower in MI+SR, but these were not significantly different between MI+V and MI+SR (Figures 8B-E).

3.4 Body and tissue weights

SR9009 treatment was reported to reduce body weight (BW) in obese mice fed with a high-fat diet (Laura et al., 2012); however, there was no significant difference in BW between MI+V and MI+SR before and after the procedure (Figure 9A). Moreover, the ratio of LV weight to BW and the ratio of lung weight to BW were not significantly different between MI+V and MI+SR (Table, Figures 9B-C).

	Sham+V n=4	Sham+SR n=4	MI+V n=9	MI+SR n=7
BW (g)	24.02±0.62	25.35±0.23	23.77±0.75	23.39±0.83
LV/BW(mg/g)	4.29±0.05	4.44±0.15	5.42±0.36*	5.35±0.51*
Lung/BW (mg/g)	5.38±0.21	5.19±0.13	8.25±1.08*	7.20±0.87*
LVDd (mm)	3.16±0.19	2.78±0.24	5.25±0.21*	4.88±0.26*
LVDs (mm)	2.13±0.23	1.87±0.30	4.97±0.24*	4.36±0.30*
FS (%)	31.67±4.74	32.29±4.10	6.23±0.92*	11.07±2.04*†
EF (%)	64.67±7.66	61.71±6.27	13.85±2.02*	23.78±4.21*†
IVST (mm)	0.725±0.02	0.69±0.11	0.67±0.06	0.74±0.03
PWT (mm)	0.62±0.10	0.90±0.07	0.68±0.04	0.60±0.11
LV Mass (mg)	83.12±12.11	85.72±11.72	156.02±21.33*	147.30±11.64*

Table. Tissue weights and echocardiographic analysis.
The values are mean ± SD. (n=4 in each sham group, n=9 animals in

MI+V group, and n=7 animals in MI+SR group). *p<0.05 vs Sham+V; †p<0.05 vs MI+V.

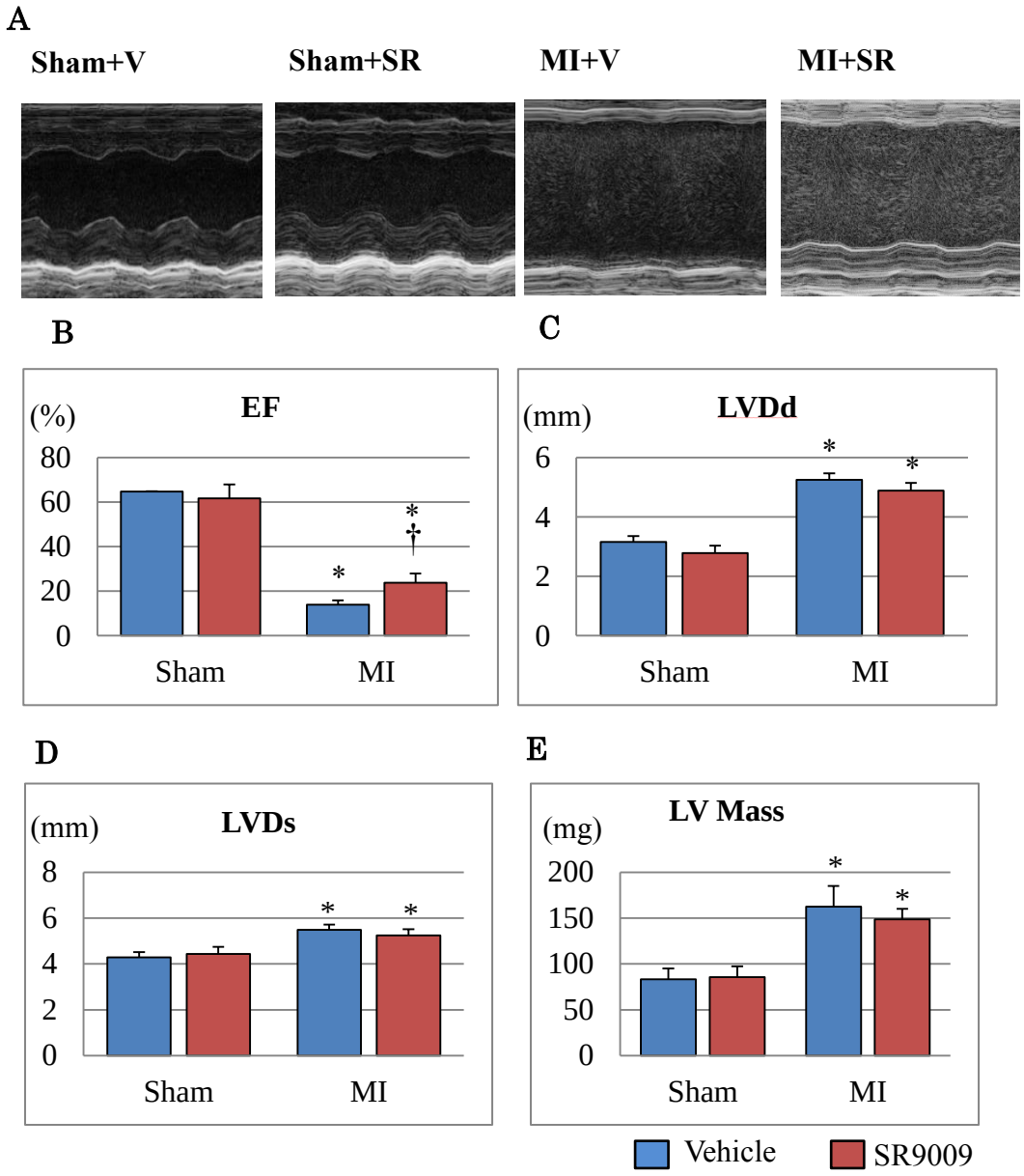

Figure 8 Echocardiographic analysis.
(A) The representative M-mode findings of echocardiography 7 days after MI. LV ejection fraction (EF) (B) was significantly higher in MI+SR than in MI+V, whereas LV end-diastolic diameter (LVDd) (C), LV end-systolic diameter (LVDs) (D) and LV mass (E) were not significantly different between MI+V and MI+SR (n=4 in each sham group, n=9 animals in MI+V group, and n=7 animals in MI+SR group). *p<0.05 vs Sham+V; †p<0.05 vs MI+V.

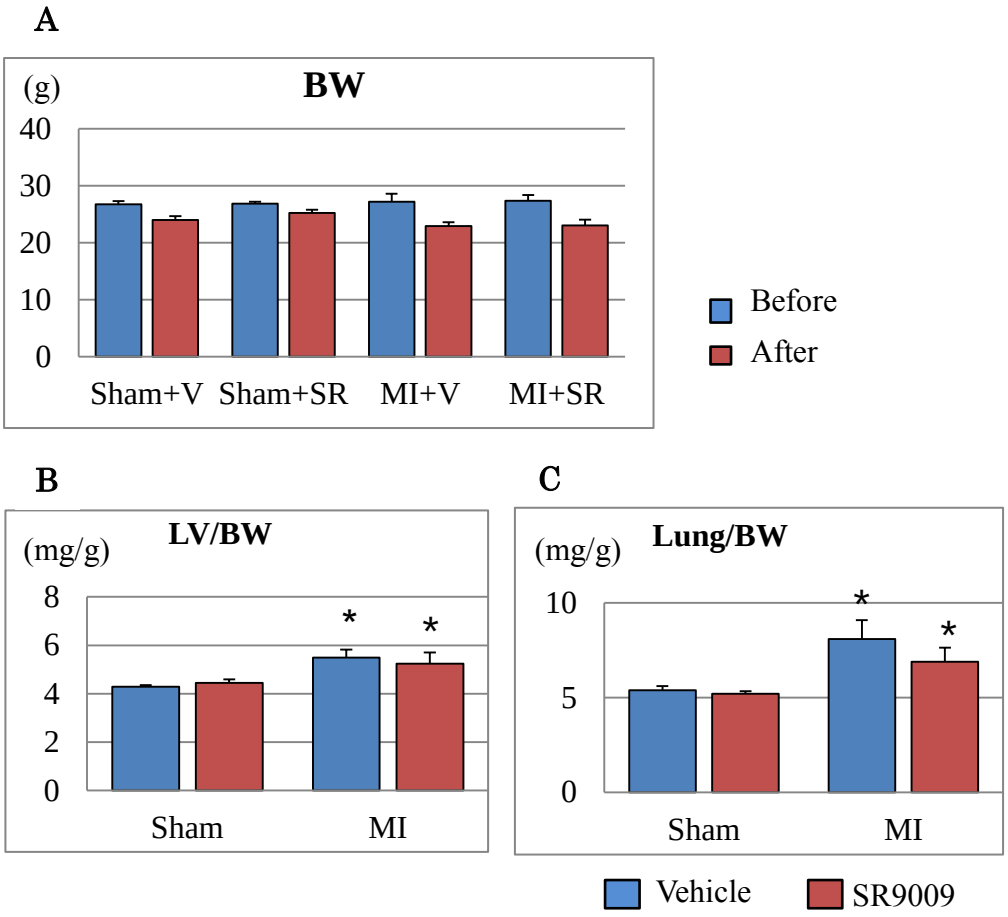

Figure 9 Body weight and tissue weight.
Body weight (BW) (A) was decreased after surgery, but not significantly different in all groups. The ratio of left ventricular (LV) weight to BW (B) and lung weight to BW (C) were also not significantly different between MI+V and MI+SR (n=4 in each sham group, n=8 animals in MI+V group, and n=7 animals in MI+SR group). The bar graphs show the group mean±SEM. *p<0.05 vs Sham+V.

3.5 Histology and collagen deposition

LV size and wall thickness were similar between Sham+V and Sham+SR.

Although collagen deposition was observed in large areas of the LV of both

MI+V and MI+SR, there were no obvious histological differences between the two groups (Figures 10A-D). Quantitative analysis revealed that there was no significant difference in collagen depositing area between MI+V and MI+SR (Figure 10E) LV gene expression levels of *Col1a* and *Col3a* were markedly upregulated 7 days after MI. SR9009 treatment reduced the *Col1a* expression, but there were no significant differences in mRNA expression levels of *Col1a* and *Col3a* between MI+V and MI+SR (Figures 10F-G).

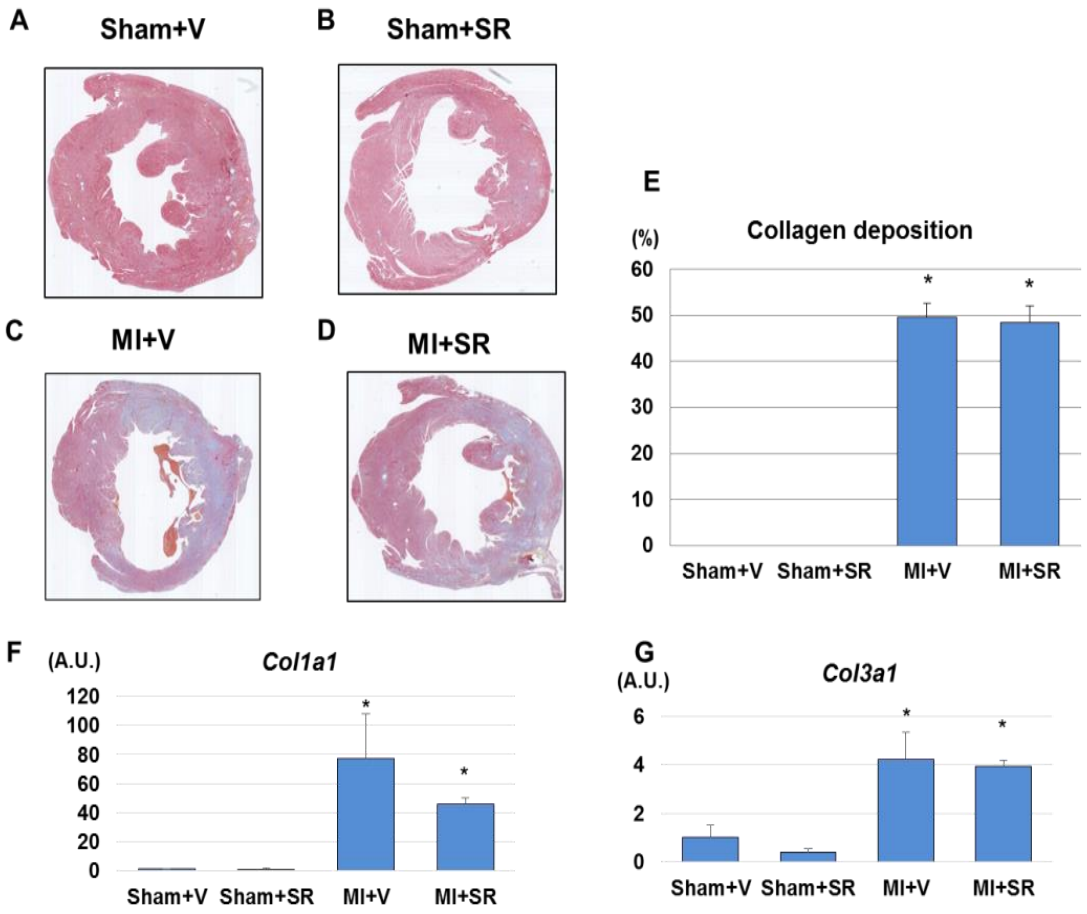

Figure 10. Collagen deposition.
Representative photomicrographs of the left ventricles at papillary

muscle level Sham+V (A), Sham+SR (B), MI+V (C), and MI+SR (D). (E) The ratio of collagen depositing area to total area. There was no significant difference in collagen deposition between MI+V and MI+SR (n=4 animals in each group). (F) The mRNA expression level of collagen type Ia1 (*Col1a*) was significantly increased in MI+V, and was tend to be decreased in MI+SR, but not significantly different between MI+V and MI+SR. (G) The mRNA expression level of collagen type IIIa1 (*Col3a*) was also significantly increased in MI+V, and was not significantly different between MI+V and MI+SR (n=4 animals in each group). *p<0.05 vs Sham+V. Scale bar (1.02 mm)

3.6 Real-time PCR of gene expressions and plasma BNP concentration analysis

We next investigated mRNA expression levels on 3 and 7 days after MI in the LV by using real-time PCR. The mRNA expression level of natriuretic peptide precursor B (*Nppb)*, which encodes a marker of heart failure brain natriuretic peptide, was 8-fold higher in MI+V compared to Sham+V, and it was significantly lower in MI+SR than in MI+V. Moreover, the left ventricular expression levels of inflammatory cytokines *Il6* and *Mcp1*, neutrophil-related surface antigen *Ly6g*, and monocyte/macrophage-related surface antigen *Cd11b* were increased after MI, and these levels were dramatically decreased by SR9009 treatment. The mRNA expression levels of *Mmp9*, a major extracellular matrix protein playing a critical role in post-MI remodeling, was also increased in MI+V and was significantly

decreased in MI+SR compared with MI+V. Moreover, plasma BNP concentration on day 7 was also significantly higher in MI+V than in Sham+V, and it was significantly lower in MI+SR than in MI+V. These results suggested that infiltration of neutrophils and monocytes/macrophages, and productions of inflammatory cytokines and extracellular matrix were reduced by the treatment with SR9009 during the acute phase of MI (Figures 11-12).

It has been reported that Rev-erb α regulates not only inflammation but also metabolic process. Rev-erb α controls mitochondrial biogenesis and respiration in the skeletal muscle through the AMPK-SIRT1-PGC-1α-TFAM signaling pathway. However, we could not find significant increases in the expression level of *Tfam1*, a gene encoding mitochondrial transcriptional factor A, and also in the expression levels of *Ppara, Pgc1*, genes encoding key enzymes of fatty acid metabolism; *Pdk4, Glut4*, genes encoding key enzymes of glucose metabolism; and *Bdh1*, a gene encoding of ketone metabolism, between MI+V and MI+SR 7 days after MI (Figure 13).

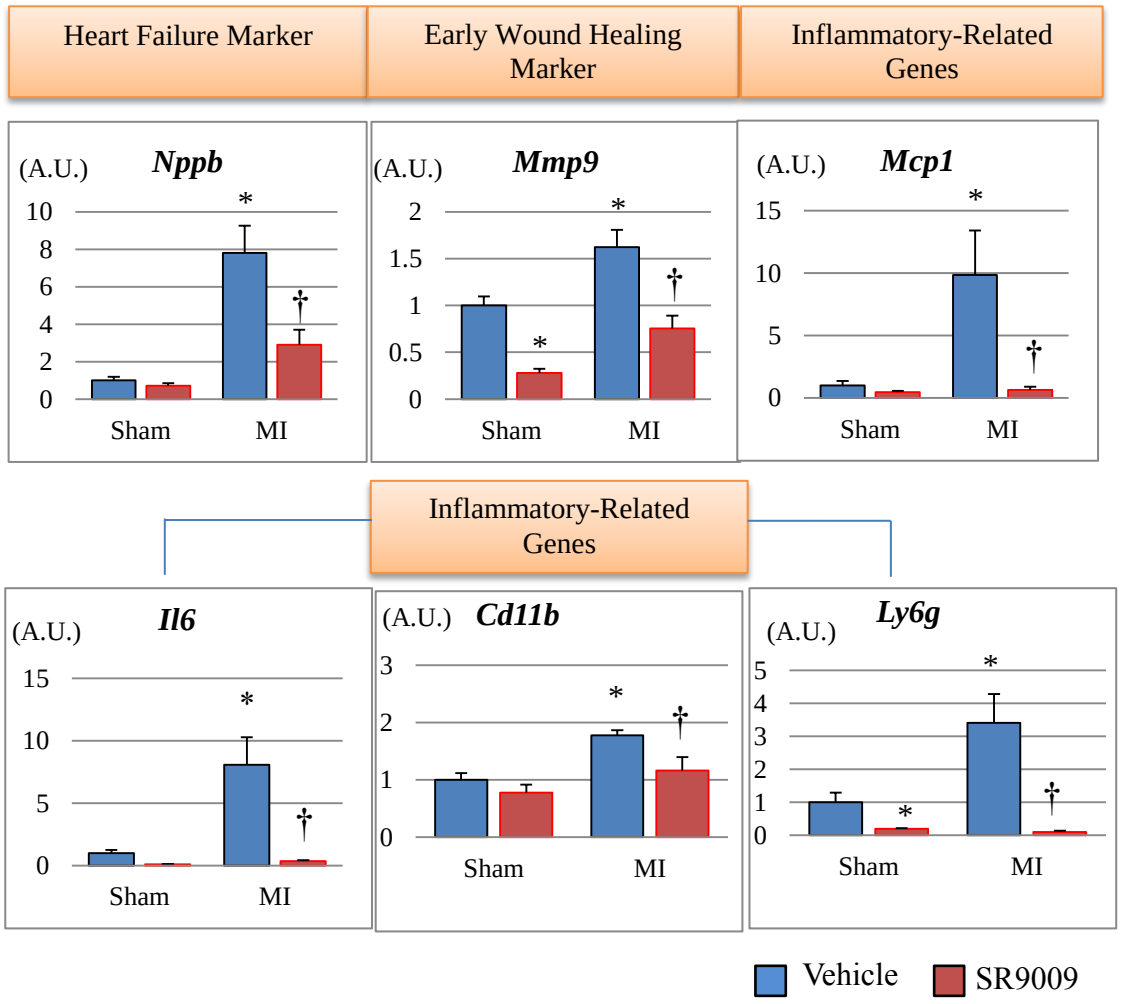

Figure 11. Gene expression levels of the left ventricles analyzed by real-time PCR on days 3.
The mRNA expression level of natriuretic peptide precursor B (*Nppb*) was significantly lower in MI-SR than in MI-V (n=4 animals in each group). The expression levels of *Il6, Mcp1, Ly6g,* and *Cd11b* were significantly increased in MI+V and were markedly decreased in MI+SR. Matrix metallopeptidase *(Mmp)9* was also significantly lower in MI-SR than in MI-V. The bar graphs show the group mean±SEM. **p*<0.05 vs Sham+V; †*p*<0.05 vs MI+V.

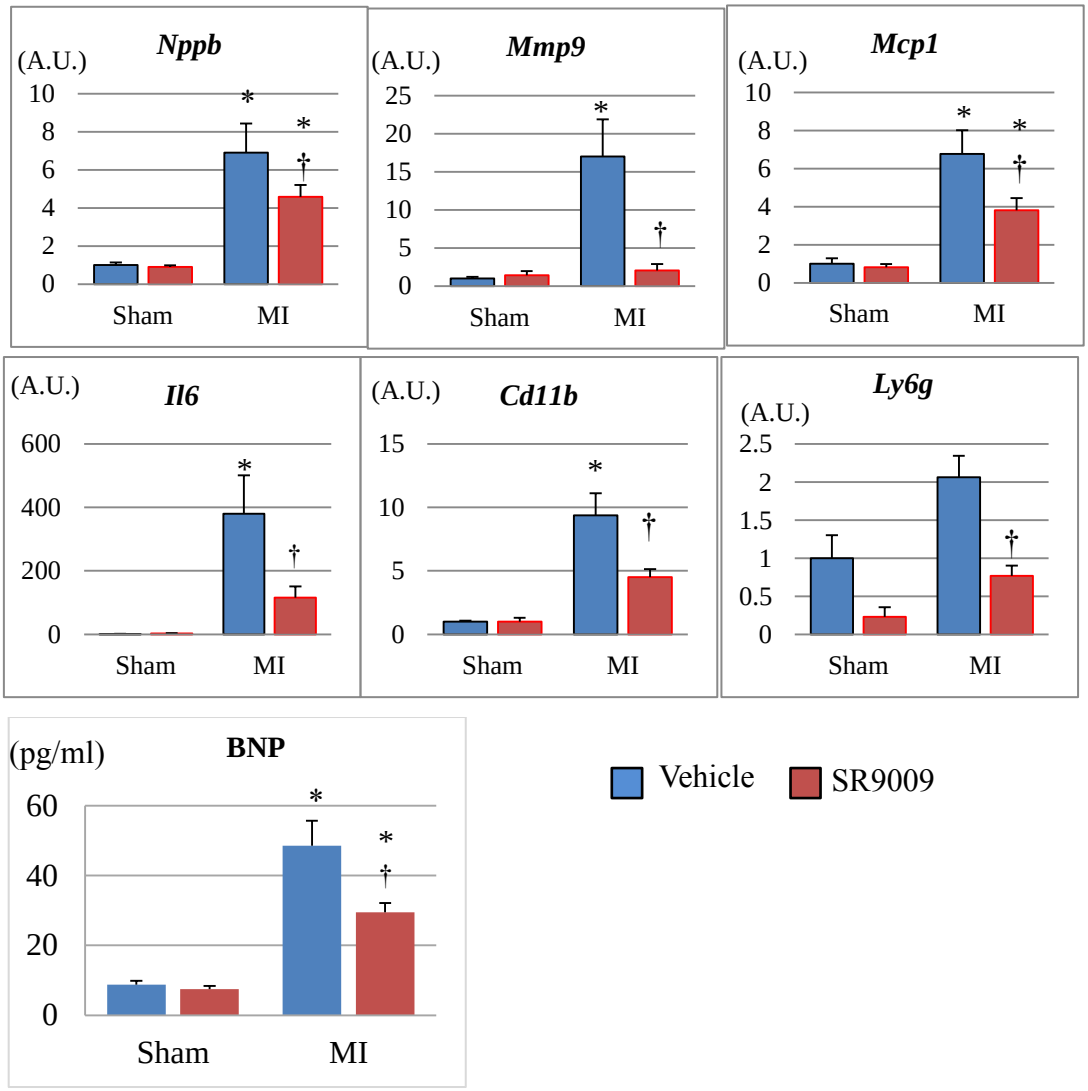

Figure 12. Gene expression levels of the left ventricles and plasma BNP concentration analyzed on days 7.

The mRNA expression level of natriuretic peptide precursor B (*Nppb*) was significantly lower in MI-SR than in MI-V (n=4 animals in each group). The expression levels of *Il6*, *Mcp1*, *Ly6g*, and *Cd11b* were significantly increased in MI+V and were markedly decreased in MI+SR. Matrix metallopeptidase *(Mmp)9* was also significantly lower in MI-SR than in MI-V. Moreover, Plasma BNP concentration was also significantly higher in MI than in sham, and was significantly lower in MI+SR than in MI+V. The bar graphs show the group mean±SEM. *p<0.05 vs Sham+V; †p<0.05 vs MI+V.

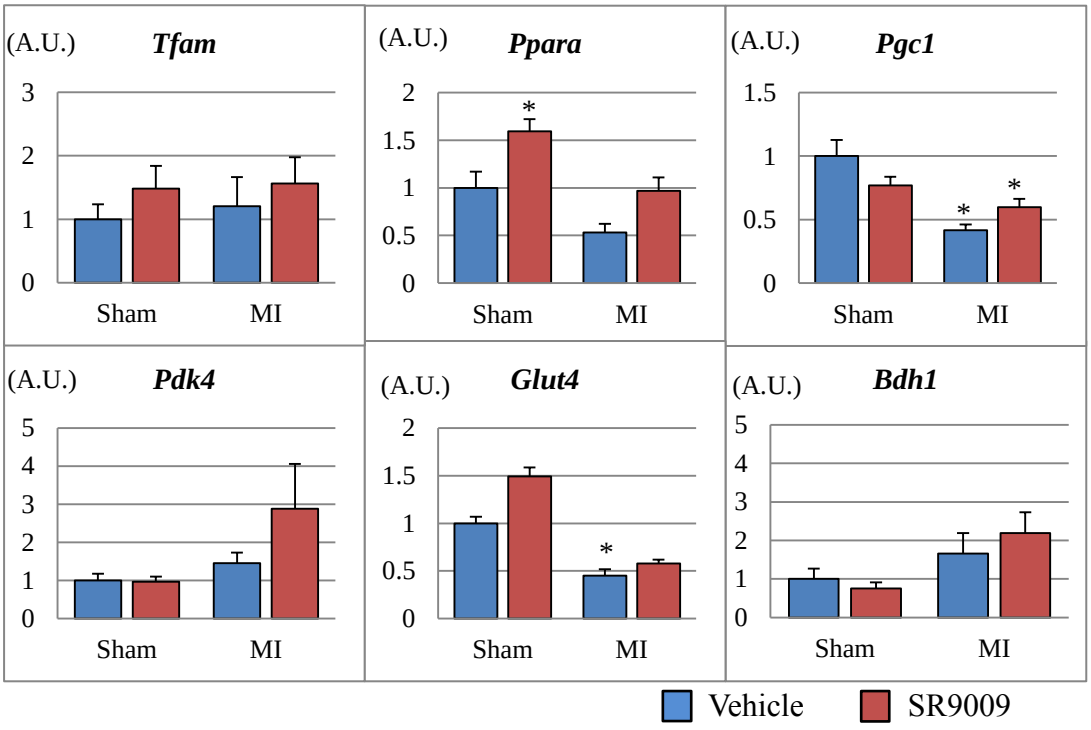

Figure 13. Metabolism-related gene expression levels of the left ventricles analyzed by real-time PCR.
There were no significant increases in the expression level of *Tfam1*, a marker of mitochondrial biogenesis, and also *Ppara*, *Pgc1*, *Pdk4, Glut4, Bdh1*, the genes encoding key enzymes of fatty acid, glucose, and ketone metabolism, between MI+V and MI+SR 7 days after MI. The bar graphs show mean±SEM. *p<0.05 vs Sham+V.

3.7 Immunofluorescence for Rev-erb α and MMP9

To confirm the protein expression level of Rev-erb α and MMP9 after MI, we performed immunofluorescence. Immunofluorescence for Rev-erb α showed that green fluorescence-positive nuclei could be detected mainly in the cardiomyocytes, and it was reduced after MI (Figure 14).

Immunofluorescence intensity for MMP9 could be weakly detected in both of the sham groups, and it was enhanced mainly in the interstitial tissue of the border area after MI. MI+SR displayed less intensity of MMP9 compared to that in MI+V (Figure 15). Quantitative analysis revealed that significant increase in immunofluorescence-positive area in MI+V was reduced by SR9009 treatment.

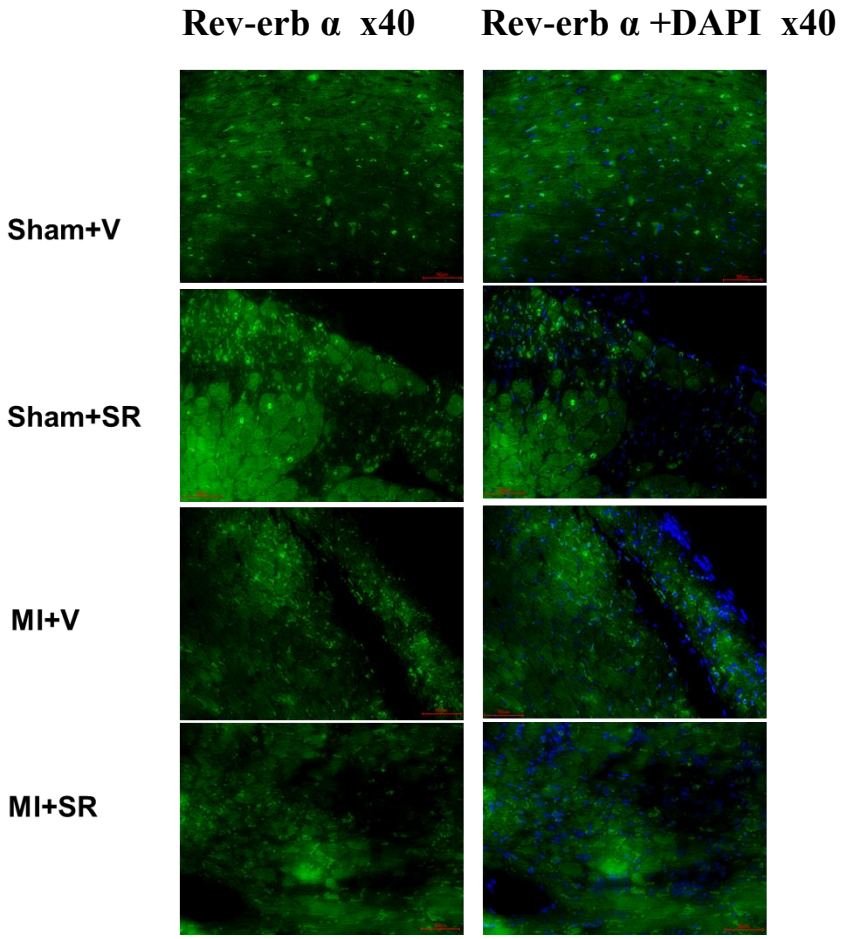

Figure 14. Representative immunofluorescence images of the left ventricles stained with Rev-erb α.
Rev-erb α was stained with Alexa Fluor 488 (green), and nuclei were stained with DAPI (blue). All images show 40× magnification. Scale bar (50 μm).

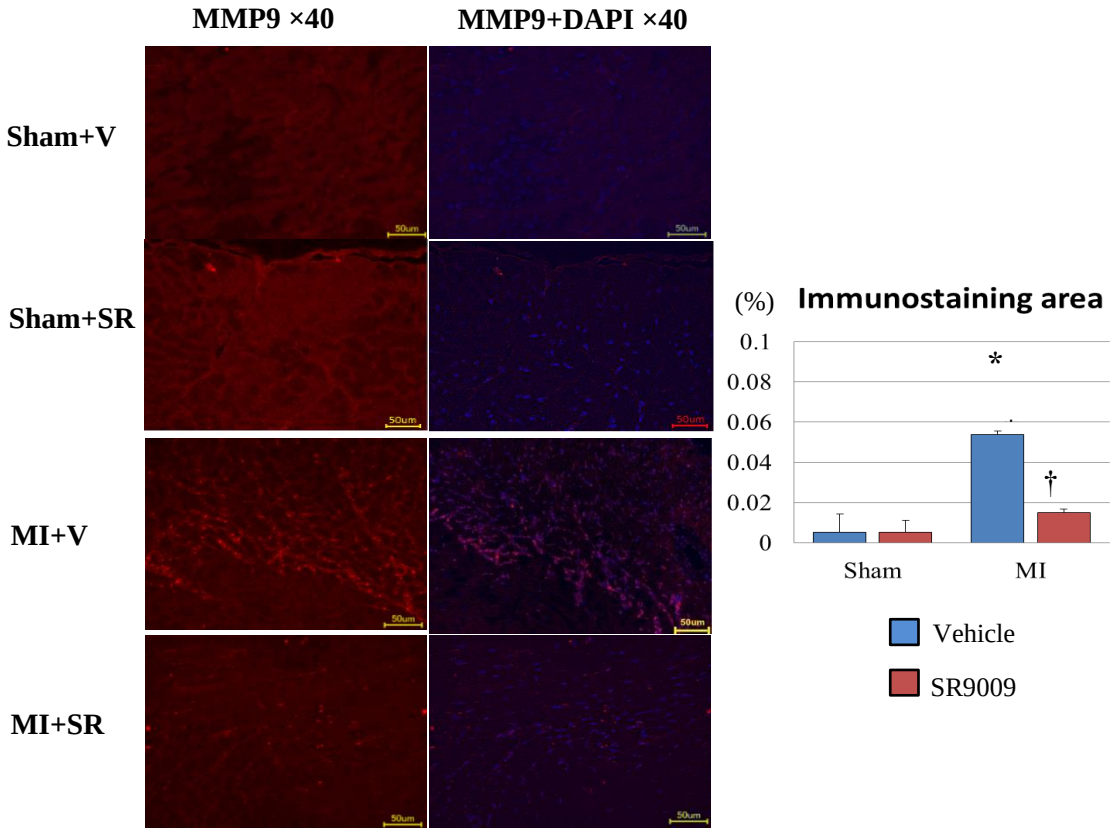

Figure 15. Representative immunofluorescence images of the left ventricles stained with MMP9.
MMP9 was stained with Alexa Fluor 594 (red), and nuclei were stained with DAPI (blue). All images show 40× magnification. The ratio of immunofluorescence-positive area to total area was significantly increased in MI+V and was markedly decreased in MI+SR (n=4 animals in each group). The bar graphs show the group mean±SEM. *p<0.05 vs Sham+V; †p<0.05 vs MI+V. Scale bar (50 μm)

3.8 Flow cytometry analysis of inflammatory cell infiltration in the LV

To further investigate the effect of SR9009 on the infiltration of inflammatory cells into the LV during the acute phase of MI, we performed flow cytometric analysis. $CD45^+CD11b^+Ly6G^+$ cells (neutrophils) were dramatically increased in the heart 1 day after MI from MI+V compared to Sham+V. SR9009 treatment decreased the infiltrations of $CD45^+CD11b^+Ly6G^+$ cells 1 day after MI. Quantitative analysis revealed a significant decrease in the percentage of $CD45^+CD11b^+Ly6G^+$ cells to $CD45^+$ cells. These results suggested that neutrophil influx was reduced by the treatment with SR9009 during the acute phase.

This study next investigated the infiltrations of M1/M2 macrophages in the heart 5 days after MI. The percentage of $CD11b^+F4/80^+CD206^+$ cells (M2 macrophages) to live cells was not significantly different between MI+V and MI+SR 5 days after MI; however, the percentage of $CD11b^+F4/80^+CD206^-$ cells (M1 macrophages) to live cells was significantly lower in MI+SR than in MI+V (Figure 16).

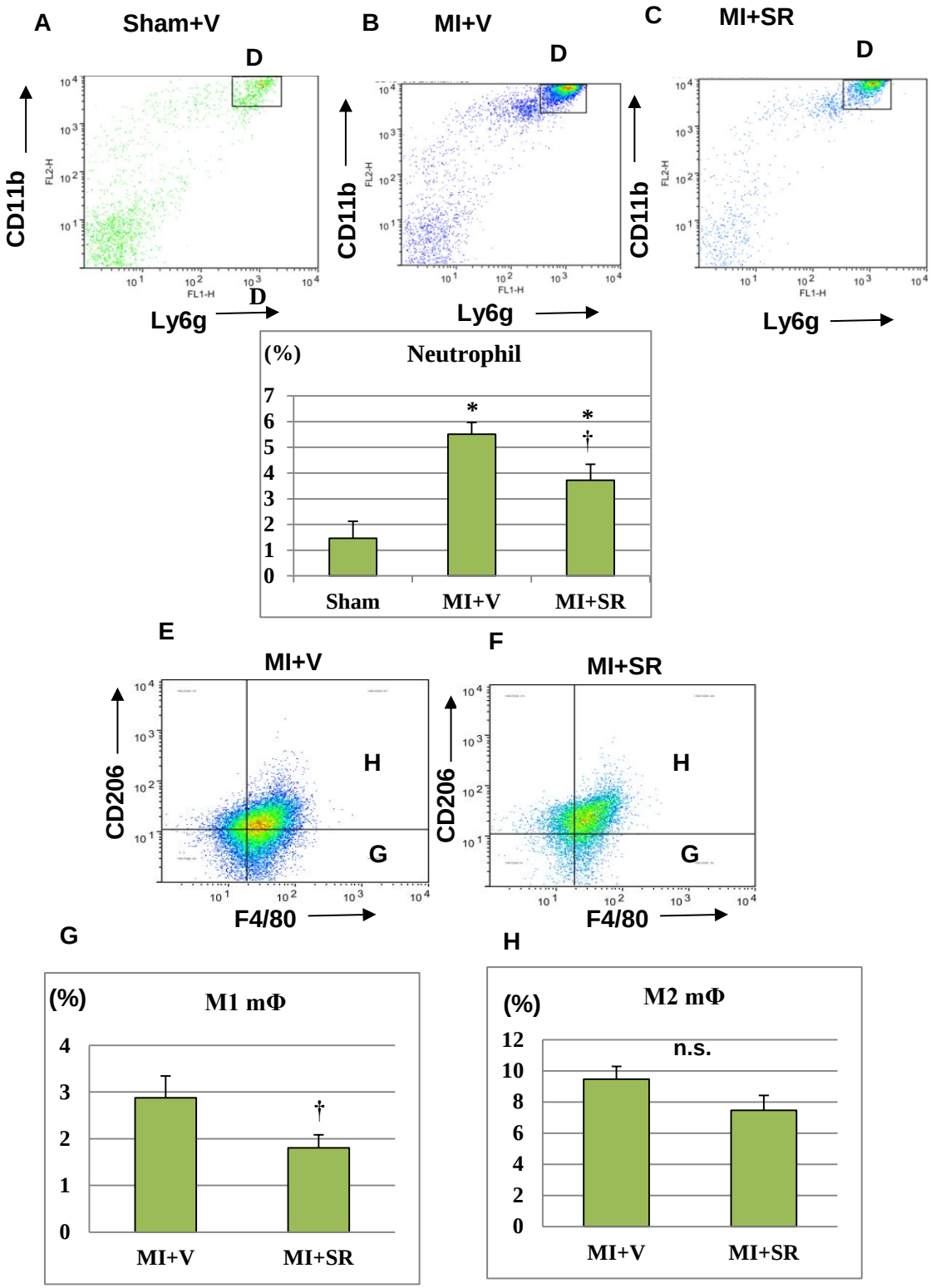

Figure 16. Flow cytometric analysis.
Flow cytometric analysis of the infiltration of inflammatory cells into the infarct and border areas at 1 day after myocardial infarction (MI)

(n=5 in each group). The representative plots (gated on $CD45^+$ and expanded into Ly6G and CD11b) of Sham+V (A), MI+V (B), and MI+SR9009 (C) are shown. The percentage of $CD45^+CD11b^+Ly6G^+$ cells (neutrophils) (D) to $CD45^+$ cells was significantly lower in MI+SR than in MI+V, suggesting that neutrophil infiltration was reduced by SR9009 treatment. (E-G) Flow cytometric analysis of M1/M2 macrophage infiltration into the infarct and border areas at 5 days after MI (n=5 in each group). The representative plots (gated on CD11b and expanded into F4/80 and CD206) of MI+V, and MI+SR9009 are shown. The percentage of $F4/80^+CD206^-$ cells to live cells was significantly lower in MI+SR than in MI+V although the percentage of $F4/80^+CD206^+$ cells to live cells was not significantly different between MI+V and MI+SR, suggesting that proinflammatory M1 macrophage infiltration was reduced by SR9009 treatment. The bar graphs show the group mean±SEM. *p<0.05 vs Sham+V; †p<0.05 vs MI+V.

3.9 Western blotting for NF-κB and MAPKs signaling

Rev-erb α has been reported to repress cytokine productions not only directly through a Rev-erb α-binding motif but also indirectly through NF-κB and/or MAPK-signaling pathway (Sato et al., 2014a; Sato et al., 2014b). Therefore, we performed western blotting to evaluate whether SR9009 treatment influenced NF-κB and MAPKs in the LV after MI. SR9009 treatment suppressed the expression of serine 468-phosphorylated (S468) and serine 536-phosphorylated (S536) NF-κB p65 (Figure 17A). Quantitative analysis revealed that the ratio of phospho-NF-κB p65 (S468) to NF-κB p65 was significantly lower in MI+SR than in MI+V (Figure 17B). SR9009 treatment also suppressed phosphorylations of p38 and

p44/42 (ERK) (Figure 17A). The ratios of phosphorylated p38 to p38 and phosphorylated ERK to ERK were significantly lower in MI+SR than in MI+V (Figure 17D).

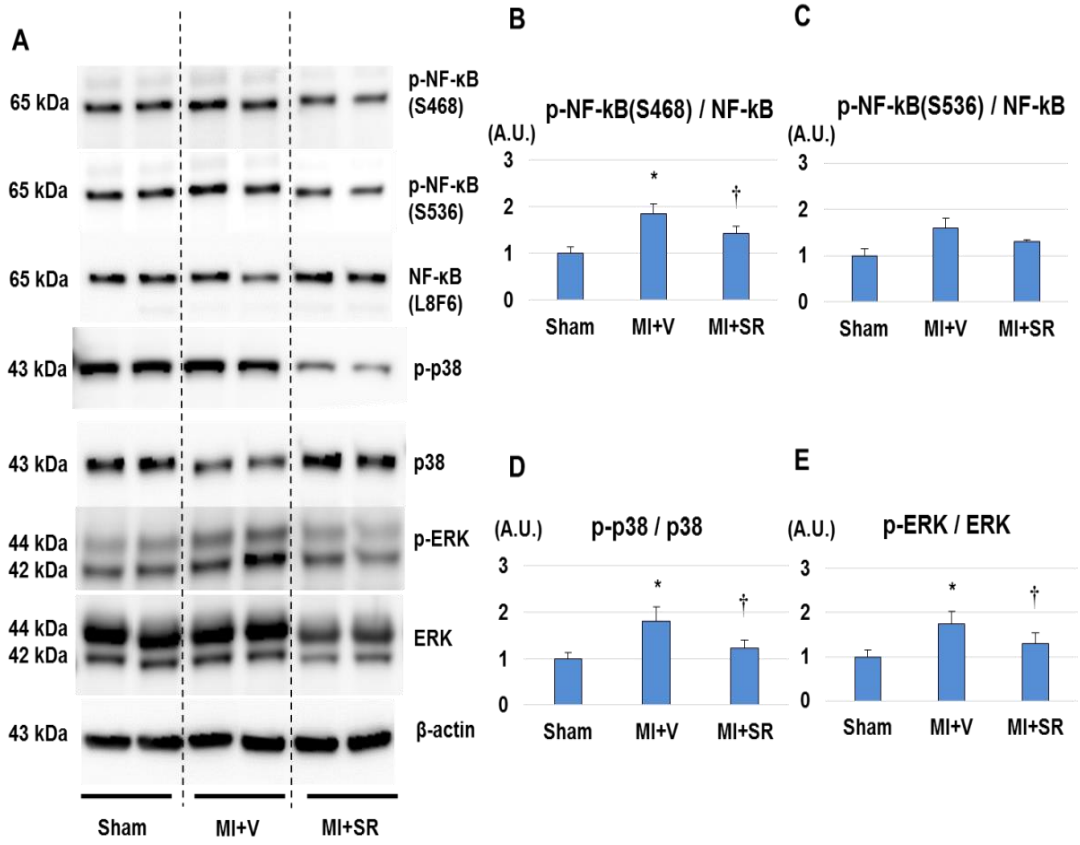

Figure 17. Western blotting analysis.
(A) Representative images of western blotting for phospho-NF-κB p65 (S468 and S536), NF-κB, phospho-p38, p38, phospho-ERK, ERK, and β-actin. (B) The ratio of phospho-NF-κB (S468) to NF-κB was significantly lower in MI+SR than in MI+V. (C) The ratio of phospho-NF-κB (S536) to NF-κB had a similar tendency, but no significant difference. (D) The ratio of phospho-p38 to p38 was significantly lower in MI+SR than in MI+V. (E) The ratio of phospho-ERK to ERK was also significantly lower in MI+SR than in MI+V. (n=3 animals in each group). The bar graphs show the group mean±SEM. *p<0.05 vs Sham+V; †p<0.05 vs MI+V.

Chapter 4 Discussion

In this study, we showed for the first time, to our knowledge, that Rev-erb agonist SR9009 improved LV function and survival after MI. Moreover, we also showed that Rev-erb agonist decreased *Il6* and *Mcp1* production, *Mmp9* expression, NF-κB and MAPKs activations, and neutrophil/M1 macrophage infiltrations in infarct and border myocardium during the acute phase of MI. These results suggested that the pharmacological activation of Rev-erb exerts beneficial effects on the acute process of post-MI remodeling by strongly inhibiting cytokine production and inflammatory cell infiltration into the infarcted heart.

Inflammatory response after MI is a double-edged sword, and how to regulate inflammation to prevent adverse cardiac remodeling is an important issue to be considered when developing a new treatment for heart failure (Anzai, 2013; Cohn et al., 2000; Weiford, 2005). In the present study, we showed that the expression levels of inflammatory cytokines including *Mcp1* and *Il6* were dramatically suppressed by SR9009 treatment in the LV during the acute phase of MI, and that of *Mmp9* was also suppressed by SR9009 treatment. Moreover, we also showed that NF-κB

and MAPKs activation were inhibited by the treatment with SR9009. These findings are consistent with the previous studies (Gibbs et al., 2011; Lam et al., 2013; Sato et al., 2014a; Sato et al., 2014b). Sato et al. reported that activated Rev-erb α repressed *Il6* expression not only directly through a Rev-erb α binding motif but also indirectly through suppression of NF-κB activity (Sato et al., 2014). They also reported that Rev-erb α regulated the inflammatory function of macrophages through suppression of MCP1-activating ERK and p38 signalling pathway (Sato et al., 2014). *Il6* receptor antagonist has been reported to reduce leukocyte and macrophage infiltration and attenuate MMP activation, leading to a marked improvement in LV remodeling and survival after MI (Möllmann et al., 2010). Moreover, targeted deletion of *Mcp1* attenuated LV remodeling after MI through decreases in macrophage infiltration and MMP activation (Dewald et al., 2005; Kaikita et al., 2004). MMP9 is known as a major subtype of metalloproteinase and plays a crucial role in post-MI remodeling. In the acute inflammatory phase after MI, neutrophils and monocytes are considered to be the predominant source of MMPs. Higher production of MMPs is more likely to cause LV wall thinning and dilatation, consequently leading to heart failure and cardiac rupture. It has been reported that genetic and pharmacological deletion of *Mmp9* prevents

adverse LV remodeling after MI (Ducharme et al., 2000; Romanic et al., 2002). Moreover, previous study reported that Rev-erbs repressed *Mmp9* expression at a distance by regulating enhancer-directed transcription (Lam et al., 2013). Thus, the present study, taken together with the findings of previous reports, suggests that the strong inhibitory effect of SR9009 on the production of inflammatory cytokines such as *Il6* and *Mcp1* attenuates neutrophil and M1 macrophage infiltrations and *Mmp9* production, at least partially through suppression of NF-κB, ERK, or p38 signalling pathway, leading to inhibition of the vicious circle of inflammatory amplification, the development of adverse LV remodeling, and cardiac rupture (Figure 18).

MAPKs are known as important signaling pathway that regulates cell survival, apoptosis, and proliferation. In the present study, phosphorylated ERK and phosphorylated p38 were significantly decreased by SR9009 treatment in the LV after MI. ERK activation is thought to inhibit apoptotic loss of cardiomyocytes and promote cardiac fibrosis. On the other hands, p38 activation has been implicated in the progression of apoptosis and cardiac dysfunction, leading to pathological remodeling although still controversial (Yeh et al., 2010).

Despite a significant improvement of LV function by SR9009 treatment, there was no significant difference in collagen deposition

between MI+V and MI+SR. The size of collagen deposition area is mainly determined by the size of the necrotic area, the wound healing response, and chronic remodeling (Kempf et al., 2012). Among them, the size of the necrotic area is the most critical for determination of the scar size in acute phase of MI, especially without reperfusion. Because we employed mice model with the permanent ligation of the proximal LAD in this study, necrotic area was relatively extensive and generally constant in each mouse. Therefore, the area of collagen deposition was mostly influenced by the size of necrotic area with or without treatment. However, because histologically-analyzing data were obtained from the samples collected within 1 week after MI, further studies are needed to evaluate the effect of Rev-erb agonist in collagen deposition in chronic phase of MI.

Rev-erb α regulates not only inflammation but also mitochondrial content and oxidative capacity. It has been reported that expression levels of phosphorylated AMPK, SIRT1, PGC1α, and mitochondrial transcription factor A (TFAM) were significantly lower in the skeletal muscle from homogenous *Nr1d1*-knockout (*Nr1d1*$^{-/-}$) mice compared to wild-type mice (Woldt et al., 2013). Consequently, mitochondrial DNA content was significantly lower in skeletal muscle from *Nr1d1*$^{-/-}$ mice, and VO_2 max during exercise was significantly lower in *Nr1d1*$^{-/-}$ than in wild-type mice.

By contrast, pharmacological activation or skeletal muscle-specific *Rev-erb α* overexpression resulted in the opposite phenotypes. These findings suggest that Rev-erb α controls mitochondrial biogenesis and respiration in the skeletal muscle through the AMPK-SIRT1-PGC1α-TFAM signaling pathway. Several studies reported that activation of AMPK, such as treatment with metformin, protects the heart against cardiac stress such as ischemia by regulating glucose and fatty acid metabolism (Susheel et al., 2007; Whittington et al., 2013). Therefore, favorable effects of Rev-erb agonist SR9009 on cardiac function may be partially attributed to activation of this pathway and modulation of the metabolic process (Jaramillo et al., 2010; Joseph Bass, 2010; Ramakrishnan et al., 2005; Raspé et al., 2002; Yang et al., 2013). However, we could not find significant increases in the expression levels of mitochondrial biogenesis-related gene and key enzymes of cardiac metabolism between MI+V and MI+SR 7 days after MI. Because mitochondrial respiration is bound to be strongly suppressed under ischemic conditions during the acute phase of MI, the result seems inevitable to maintain energy metabolism during the acute phase of MI. Further studies are needed to clarify the effect of the Rev-erb agonist on cardiac metabolism after MI, especially during the chronic phase.

SR9009 and SR9011 were synthesized as novel Rev-erb agonists, and they have been reported to improve hyperglycemia, dyslipidemia, and skeletal muscle oxidative capacity by modulating mitochondrial number and oxidative function in mice (Woldt et al., 2013). Moreover, long-term treatment with SR9009 could reduce atherosclerotic plaque by decreasing the ratio of pro-inflammatory M1 macrophages to anti-inflammatory M2 macrophages in LDL receptor-deficient mice fed a Western diet (Sitaula et al., 2015). The present study showed no apparent toxicity in consistent with previous study (Sitaula et al., 2015) Although we administered only one dose of SR9009 (100 mg/kg/day) intraperitoneal according to the previous study (Sitaula et al., 2015; Solt et al., 2012), we may need another dose to investigate whether dose dependency exists. Moreover, we tried to start the treatment with SR9009 on the next day after MI surgery; however, the survival rate and LV function did not reach significant improvement. Longer periods of severe ischemia (usually more than 6-hour ischemia due to complete coronary occlusion) is considered to cause loss of most cardiomyocytes in the subendocardial region of the ischemic area (Frangogiannis, 2015). “Late-start treatment” with SR9009 may not exert enough inhibitory effects on cardiac cell death although a single injection of 100 mg/kg of SR9009 quickly alters circadian pattern and metabolic

gene expressions in mice (Solt et al., 2012). Recently, Zhang et al reported that SR9009 ameliorated norepinephrine-induced cardiomyocyte hypertrophy, pressure-overloaded cardiac hypertrophy and heart failure in mice through transcriptional repression of the fetal gene program. They also showed a protective effect of SR9009 for the endothelin-1–induced hypertrophy using human induced pluripotent stem cell-differentiated cardiomyocytes (iPS-CM), just as in the rodent cardiomyocytes (Zhang et al., 2017). Thus, Rev-erb agonist has a direct protection in the cardiomyocytes in a cell-autonomous fashion, consistent with our results. As clinical implications, Rev-erb agonists may be useful for secondary prevention in patients with prior MI or metabolic syndrome with high risk for coronary artery disease although late-start treatment with Rev-erb agonist after the onset of MI may not be enough to improve clinical prognosis.

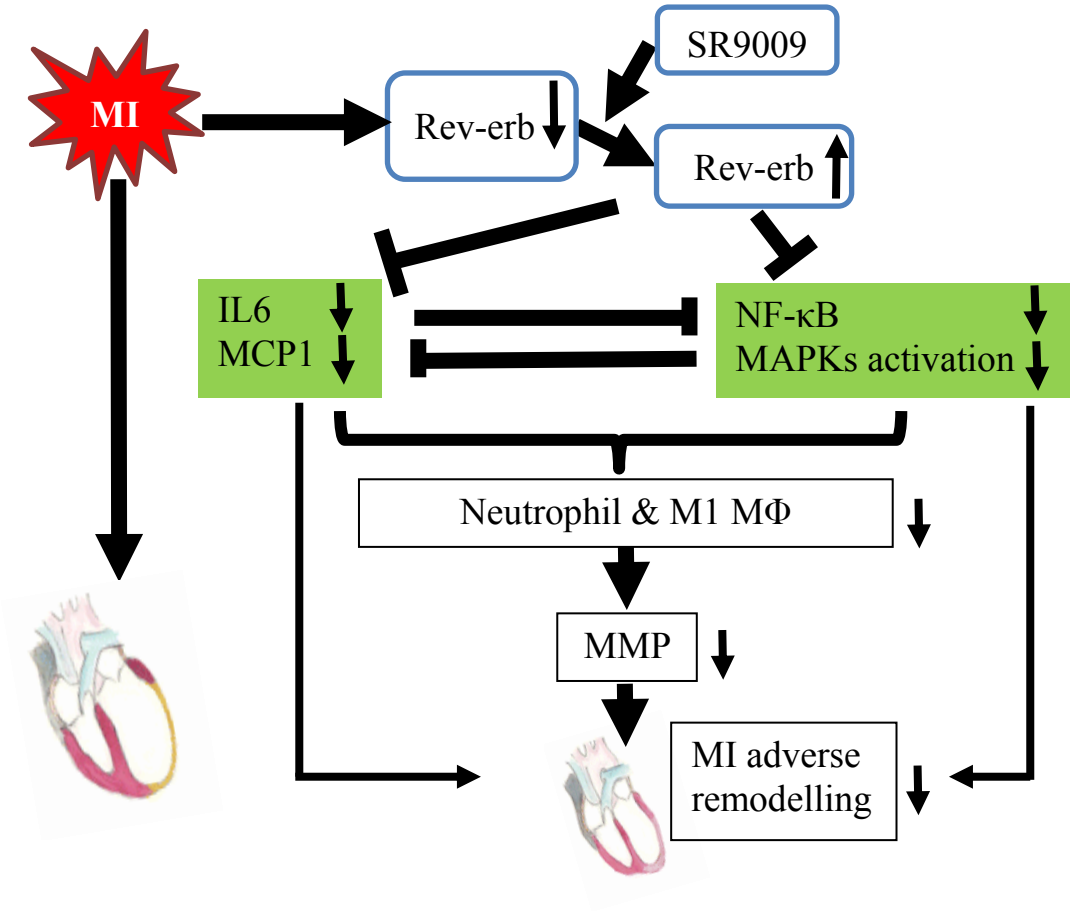

Figure 18. Schema of action of Rev-erb on post-MI remodeling.
This schema shows possible roles of Rev-erb in post-MI remodeling. The strong inhibitory effect of SR9009 on the production of inflammatory cytokines such as IL6 and MCP1 attenuates neutrophil and M1 macrophage infiltrations and MMP9 production, at least partially through suppression of NF-κB, ERK, or p38 signalling pathway, leading to inhibition of the development of adverse LV remodeling, and cardiac rupture. However, the decreasing of IL-6 and MCP-1 productions or NFkb and mapks activation independently also may directly inhibit post MI remodeling.

Chapter 5 Clinical Implications

In terms of clinical implications, the present study, taken together with the previous reports, suggested that Rev-erb agonists can be expected to be promising novel drugs not only for metabolic syndrome and atherosclerotic disease but also for MI and heart failure. For example, the drugs may be useful for secondary prevention in patients with MI complicated with metabolic syndrome.

Chapter 6 Study Limitation

The present study included the following limitations. First, we only studied the acute phase of MI using a mouse model with permanent ligation of the coronary artery. Further studies are needed to elucidate the long-term effects of Rev-erb agonist and/or in an ischemia/reperfusion model. Second, although we administered only one dose of SR9009 (100 mg/kg/day) according to the previous study and displayed no apparent toxicity (Sitaula et al., 2015; Solt et al., 2012), we may need another dose to investigate whether dose dependency exists. Third, recent study did not check the SR9009 tissue concentration or the distribution in the tissue. Fourth, this study suggested that the favorable effect of SR9009 on post-MI remodeling was mainly attributed to the strong attenuations of inflammatory cytokine production and MMP9 production. However, another mechanism such as alteration of metabolic processes and/or circadian rhythm may contribute to the results. Further studies are desirable to investigate the mechanism of the effect of Rev-erb activation on post-MI remodeling using antagonist or gene-manipulated mice models.

Chapter 7 Conclusions

In conclusion, Rev-erb agonist SR9009 could improve cardiac function and survival in a mouse model of acute MI by inhibiting cytokine production and inflammatory cell infiltration. Rev-erb α is expected to be a promising therapeutic target not only for metabolic syndrome and atherosclerotic disease but also for MI and heart failure.

Acknowledgements

Praise to be God for my doctoral thesis, while the crowning moment of several years of hard work. This dissertation is dedicated to my father-Soenarno, who passed away because of heart disease. This is also my pleasure to write some words in appreciation for all the incredible ones who were involved in my voyage of several years in Japan.

Firstly, I would like to express my gratefulness to the Almighty Allah SWT for this miracle life and for bringing all the beauty and goodness in my life.

I take this opportunity to deliver my gratitude to my supervisor Professor Kazutaka Aonuma for all the precious kindness, guidance, and support during my study. He always helps his students and cares about their daily life. His attention, moral support and timely suggestions were always inspired me. Thank you for giving me the opportunity to work in his department as a graduate student.

I am indebted grateful to assistant professor Dr Nobuyuki Murakoshi that also my mentor for his excellent technical assistance, valuable instruction, guidance, support and supervision throughout my experiments in this study. This thesis would not have been possible without his help and support.

I would like also express my sincere gratefulness to Dr Tajiri K, Dr Kimura T, Dr Xu D, Dr Sakai S and all teachers in Department of Cardiology and Tsukuba University for the knowledge and the experience during my study in Japan.

My sincere thanks are also extended to all of my referees Professor Hiromi Yanagisawa, Dr Ken Nishimura, Dr Nobutake Shimojyo, Dr Yoshiaki Kato for their valuable suggestions, times and all of their instructive comments

that helped me to improve my dissertation.
A Special gratitude and love goes to my family for their unfailing support and their unconditional love, understanding also supports. Thank you so much for my lovely husband Hisyam Ridha Maulana for taking care of our daughter and sharing the housework during my study. He always encouraged me and helped me overcome the difficulties without complaining. Thank you also for my daughter Cassara Kindha Avariella, for her understanding and patience when she needed me most. I wish to express my sincere thanks to my lovely late father and father in law, grandfather and grandmother, for keep watching me from the heaven. I also place on my record, my sincere gratitude to my lovely mother-Endang Sri Rejeki, my parents in law and also all my big family for unceasing encouragement, prayer and support.
I also not forget to bring thank you for all my colleagues, Qin R, Feng D, Saori Y, Ogura Y, Honda sensei, Yamagami sensei and all my Indonesian friends who study and/or live in Tsukuba. It is an unforgettable moment when I knew all of you. I would like also acknowledge and thank to Mrs. Isaka Y, Mrs. Inoue S, Mrs. Miyamoto A for the technical assistance and multifarious support during my study.
Last but not least, I gratefully acknowledge to all supporter of this research, Professor Kazutaka Aonuma, Tsukuba University and Ministry of Education, Culture, Sports, Science and Technology-Japan (MEXT) for the financial support during my study in Japan.
Thank you so much again to all who have helped and support me.

Reference

Anzai, T. (2013). Post-Infarction Inflammation and Left Ventricular Remodeling. *Circulation Journal*, 77(3), 580-587. https://www.jstage.jst.go.jp/article/circj/77/3/77_CJ-13-0013/_article

Bugge, A., Feng, D., Everett, L.J., Briggs, E.R., Mullican, S.E., Wang, F., Jager, J., Lazar M.A. (2012). Rev-erba and Rev-erbb coordinately protect the circadian clock and normal metabolic function. *Genes Dev*, 26(7):657-667. https://www.ncbi.nlm.nih.gov/pmc/articles/PMC3323877/

Chambon, P. (2005). The Nuclear Receptor Superfamily : A Personal Retrospect on the First Two Decades. *Molecular Endocrinology,* 19(6), 1418-1428. https://academic.oup.com/mend/article-lookup/doi/10.1210/me.2005-0125

Cohn, J. N., Ferrari, R., & Sharpe, N. (2000). Cardiac remodeling-concepts and clinical implications: A consensus paper from an International Forum on Cardiac Remodeling. *Journal of the American College of Cardiology*, 35(3), 569-582.

http://www.sciencedirect.com/science/article/pii/S0735109799006300?via%3Dihub

Dewald, O., Zymek, P., Winkelmann, K., Koerting, A., Ren, G., Abou-Khamis, T., Michael, L. H., Rollins, B. J., Entman, M. L., Frangogiannis, N. G. (2005). CCL2/monocyte chemoattractant protein-1 regulates inflammatory responses critical to healing myocardial infarcts. *Circulation Research*, 96(8), 881-889. http://circres.ahajournals.org/content/96/8/881

Ducharme, A., Frantz, S., Aikawa, M., Rabkin, E., Lindsey, M., Rohde, L. E., Schoen, F. J., Kelly, R. A., Werb, Z.,Libby, P., Lee, R. T. (2000). Targeted deletion of matrix metalloproteinase-9 attenuates left ventricular enlargement and collagen accumulation after experimental myocardial infarction. *Journal of Clinical Investigation*, 106(1), 55-62. http://www.jci.org/articles/view/8768

Evans, R. M. (2005). The Nuclear Receptor Superfamily : A Rosetta Stone for Physiology, *Nuclear Endocrinology*, 19(6), 1429-1438. https://academic.oup.com/mend/article-lookup/doi/10.1210/me.2005-0046

Frangogiannis, N. G. (2015a). Pathophysiology of myocardial infarction. *Comprehensive Physiology*, 5(4), 1841-1875.

http://onlinelibrary.wiley.com/doi/10.1002/cphy.c150006/abstract;jsessionid=14DE9D788EA2767111981AFBFE80802E.f04t03

Frangogiannis, N. G. (2015b). The inflammatory response in myocardial injury, repair and remodeling. *Nature Review Cardiology Journal*, 11(5), 255-265. https://www.ncbi.nlm.nih.gov/pmc/articles/PMC4407144/

Gibbs, J. E., Blaikley, J., Beesley, S., Matthews, L., Simpson, K. D., Boyce, S. H., Farrow, S. N., Else, K. J., Singh, D., Ray, D. W., Loudon, A. S. I. (2011). The nuclear receptor REV-ERB α mediates circadian regulation of innate immunity through selective regulation of inflammatory cytokines. *Proceedings of the National Academy of Sciences of the United States of America*, 109(2), 582-587. https://www.ncbi.nlm.nih.gov/pmc/articles/PMC3258648/

Jaramillo, C., Ochoa, D., Contreras, L., Pagani, M., Carvajal-ortiz, H., Pratt, L. M., Krishnan, S., Cardona, A., Romero, M., Quiroz, L., Rodriguez, G., Rueda, M. J. (2010). Rev-erbα, a heme sensor that coordinates metabolic and circardian pathways. *Science*, 318:1786-1789. http://science.sciencemag.org/content/318/5857/1786.long

Joseph Bass, J. S. T. (2010). Circadian Integration of Metabolism and

Energetics. *Science*, 330(6009), 1349-1354. http://science.sciencemag.org/content/330/6009/1349

Kaikita, K., Hayasaki, T., Okuma, T., Kuziel, W. A., Ogawa, H., & Takeya, M. (2004). Targeted deletion of CC chemokine receptor 2 attenuates left ventricular remodeling after experimental myocardial infarction. *The American Journal of Pathology*, 165(2), 439-447. http://ajp.amjpathol.org/article/S0002-9440(10)63309-3/fulltext

Kempf, T., Zarbock, A., Vestweber, D., & Wollert, K. C. (2012). Anti-inflammatory mechanisms and therapeutic opportunities in myocardial infarct healing. *Journal of Molecular Medicine*, 90(4),361-369. https://link.springer.com/article/10.1007%2Fs00109-011-0847-y

Lam, M. T. Y., Cho, H., Lesch, H. P., Gosselin, D., Heinz, S., Tanaka-Oishi, Y., Benner, C., Kaikkonen, M. U., Kim, A. S., Kosaka, M., Lee, C. Y., Watt, A., Grossman, T. R., Rosenfeld, M. G., Evans, R. M., Glass, C. K. (2013). Rev-Erbs repress macrophage gene expression by inhibiting enhancer-directed transcription. *Nature*, 498(7455), 511-515. http://www.nature.com/nature/journal/v498/n7455/full/nature12209.html?foxtrotcallback=true

Liehn, E. A., Postea, O., Curaj, A., & Marx, N. (2011). Repair after myocardial infarction, between fantasy and reality: The role of

chemokines. *Journal of the American College of Cardiology*, 58(23), 2357-2362. http://www.sciencedirect.com/science/article/pii/S0735109711031457?via%3Dihub

Machino-Ohtsuka, T., Tajiri, K., Kimura, T., Sakai, S., Sato, A., Yoshida, T., Hiroe, M., Yasutomi, Y., Aonuma, K. (2014). Tenascin-C aggravates autoimmune myocarditis via dendritic cell activation and Th17 cell differentiation. *Journal of the American Heart Association*, 3(6), 1-16. http://jaha.ahajournals.org/content/3/6/e001052

Matsui, Y., Morimoto, J., & Uede, T. (2010). Role of matricellular proteins in cardiac tissue remodeling after myocardial infarction. *World Journal of Biological Chemistry*, 1(5), 69-80. https://www.wjgnet.com/1949-8454/full/v1/i5/69.htm

Möllmann, H., Nef, H. M., & Troidl, C. (2010). Editorial: "Turning the right screw": Targeting the interleukin-6 receptor to reduce unfavourable tissue remodelling after myocardial infarction. *Cardiovascular Research*, 87(3), 395-396. https://academic.oup.com/cardiovascres/article-lookup/doi/10.1093/cvr/cvq186

Ramakrishnan, S. N., Lau, P., Burke, L. J., & Muscat, G. E. O. (2005).

Rev-erbß regulates the expression of genes involved in lipid absorption in skeletal muscle cells: Evidence for cross-talk between orphan nuclear receptors and myokines. *Journal of Biological Chemistry*, 280(10), 8651-8659. http://www.jbc.org/content/280/10/8651

Raspé, E., Duez, H., Mansén, A., Fontaine, C., Fiévet, C., Fruchart, J.-C., Vennström, B., Staels, B. (2002). Identification of Rev-erb alpha as a physiological repressor of apoC-III gene transcription. *Journal of Lipid Research*, 43(12), 2172-2179. http://www.jlr.org/content/43/12/2172

Romanic, A. M., Harrison, S. M., Bao, W., Burns-Kurtis, C. L., Pickering, S., Gu, J., Grau, E., Mao, J., Sathe, G. M., Ohlstein, E. H., Yue, T. L. (2002). Myocardial protection from ischemia/reperfusion injury by targeted deletion of matrix metalloproteinase-9. *Cardiovasc Res*, 54(3), 549-558. https://academic.oup.com/cardiovascres/article/54/3/549/270293/Myocardial-protection-from-ischemia-reperfusion

Sato, S., Sakurai, T., Ogasawara, J., Shirato, K., Ishibashi, Y., Oh-ishi, S., Imaizumi, K., Haga, S., Hitomi, Y., Izawa, T., Ohira, Y., Ohno, H., Kizaki, T. (2014a). Direct and Indirect Suppression of Interleukin-6

Gene Expression in Murine Macrophages by Nuclear Orphan Receptor REV-ERBα. *The Scientific World Journal*, (2014), 685854, 1-10. https://www.hindawi.com/journals/tswj/2014/685854/

Sato, S., Sakurai, T., Ogasawara, J., Takahashi, M., Izawa, T., Imaizumi, K., Taniguchi, N., Ohno, H., Kizaki, T. (2014b). A circadian clock gene, Rev-erbα, modulates the inflammatory function of macrophages through the negative regulation of Ccl2 expression. *Journal of Immunology*, 192(1), 407-417. http://www.jimmunol.org/content/192/1/407

Sitaula, S., Billon, C., Kamenecka, T. M., Solt, L. A., & Burris, T. P. (2015). Biochemical and Biophysical Research Communications Suppression of atherosclerosis by synthetic REV-ERB agonist. *Biochemical and Biophysical Research Communications*, *460*(March), 1-6. http://www.sciencedirect.com/science/article/pii/S0006291X15005161?via%3Dihub

Solt, L. A., Wang, Y., Banerjee, S., Hughes, T., J, D., Lundasen, T., Shin, Y., Liu, J., Cameron, M. D., Noel, R., Yoo, S. H., Takahashi, J. S., Butler, A. A., Kamenecka, T. M. B. T. (2012). Regulation of circadian behaviour and metabolism by REV-ERB-α and REV-ERB-β. *Nature*,

485(7396), 123-127.
https://www.nature.com/nature/journal/v485/n7396/full/nature11030.html

Thygesen, K., Alpert, J. S., Jaffe, A. S., Simoons, M. L., Chaitman, B. R., White, H. D., (2012). Third Universal Definition of Myocardial Infarction. *Journal of the American College of Cardiology*, 60(16), 1581-1598.
http://circ.ahajournals.org/content/116/22/2634

Weiford, B. C. (2005). *Braunwald's Heart Disease: A Textbook of Cardiovascular Medicine*. *JAMA: The Journal of the American Medical Association,* (Vol. 294).
http://jamanetwork.com/journals/jama/article-abstract/201229

Wen, B., Lampe, J. N., Roberts, A. G., Atkins, W. M., Rodrigues, A. D., & Nelson, S. D. (2007). Activation of AMPK by metformin improves left ventricular function and survival in heart failure. *Circulation Research, October*, 454(1), 42-54.
https://www.ncbi.nlm.nih.gov/pmc/articles/PMC2709761/

Whittington, H. J., Hall, A. R., McLaughlin, C. P., Hausenloy, D. J., Yellon, D. M., & Mocanu, M. M. (2013). Chronic metformin associated cardioprotection against infarction: Not just a glucose lowering

phenomenon. *Cardiovascular Drugs and Therapy*, 27(1), 5-16. https://link.springer.com/article/10.1007%2Fs10557-012-6425-x

Woldt, E., Sebti, Y., Solt, L. A., Duhem, C., Lancel, S., Eeckhoute, J., Hesselink, M, K, C., Paquet, C., Delhaye, S., Shin, Y., Kamenecka, T, M., Schaart, G., Lefebvre, P., Nevière, R., Burris, T, P., Schrauwen, P., Staels, B., Duez, H. (2013). Rev-erb-α modulates skeletal muscle oxidative capacity by regulating mitochondrial biogenesis and autophagy. *Nature Medicine*, 19(8), 1039-1046. https://www.nature.com/nm/journal/v19/n8/full/nm.3213.html

Xu, D., Murakoshi, N., Igarashi, M., Hirayama, A., Ito, Y., Seo, Y., Tada, H., Aonuma, K. (2012). PPAR-ɣ activator pioglitazone prevents age-related atrial fibrillation susceptibility by improving antioxidant capacity and reducing apoptosis in a rat model. *Journal of Cardiovascular Electrophysiology*, 23(2), 209-217. http://onlinelibrary.wiley.com/doi/10.1111/j.1540-8167.2011.02186.x/abstract;jsessionid=602B15E94CDA2B95CB5285C9A63B4266.f04t02

Yang, F., Inoue, I., Kumagai, M., Takahashi, S., Nakajima, Y., & Ikeda, M. (2013). Real-time analysis of the circadian oscillation of the Rev-Erb β promoter. *Journal of Atherosclerosis and Thrombosis*, 20(3), 267-76.

http://www.ncbi.nlm.nih.gov/pubmed/23221024

Yeh, C. C., Li, H., Malhotra, D., Turcato, S., Nicholas, S., Tu, R., Zhu, B., Cha, j., Swigart P. M., Myagmar, B., Baker, A. J., Simpson, P. C., Mann, M. J. (2010). Distinctive ERK and p38 signaling in remote and infarcted myocardium during post-MI remodeling in the mouse. *Journal of Cellular Biochemistry*, 109(6), 1185-1191. http://onlinelibrary.wiley.com/doi/10.1002/jcb.22498/abstract

Zhang, L., Zhang, R., Tien, C., Chan, R. E., Sugi, K., Fu, C., Griffin, A. C., Shen, Y., Burris, T. P., Jain, M. K. (2017). REV-ERB α ameliorates heart failure through transcription repression, *JCI Insight*, 2(17), 1-13. https://www.ncbi.nlm.nih.gov/pmc/articles/PMC5621902/

参　考　論　文